Original Article

MOLECULAR METABOLISM

Protein kinase D2 modulates hepatic insulin sensitivity in male mice

Patricia Rada[1,2,*,11], Elena Carceller-López[1,2,11], Ana B. Hitos[1,2], Beatriz Gómez-Santos[3,4,12], Constanza Fernández-Hernández[5,12], Esther Rey[6], Julia Pose-Utrilla[1,7,13], Carmelo García-Monzón[6,8], Águeda González-Rodríguez[1,2,6], Guadalupe Sabio[9,10], Antonia García[5], Patricia Aspichueta[3,4,8], Teresa Iglesias[1,7], Ángela M. Valverde[1,2,]**

ABSTRACT

Objectives: Protein kinase D (PKD) family is emerging as relevant regulator of metabolic homeostasis. However, the precise role of PKD2 in modulating hepatic insulin signaling has not been fully elucidated and it is the aim of this study.

Methods: PKD inhibition was analyzed for insulin signaling in mouse and human hepatocytes. PKD2 was overexpressed in Huh7 hepatocytes and mouse liver, and insulin responses were evaluated. Mice with hepatocyte-specific PKD2 depletion ($PKD2^{\Delta Hep}$) and $PKD2^{fl/fl}$ mice were fed a chow (CHD) or high fat diet (HFD) and glucose homeostasis and lipid metabolism were investigated.

Results: PKD2 silencing enhanced insulin signaling in hepatocytes, an effect also found in primary hepatocytes from $PKD2^{\Delta Hep}$ mice. Conversely, a constitutively active PKD2 mutant reduced insulin-stimulated AKT phosphorylation. A more in-depth analysis revealed reduced IRS1 serine phosphorylation under basal conditions and increased IRS1 tyrosine phosphorylation in $PKD2^{\Delta Hep}$ primary hepatocytes upon insulin stimulation and, importantly PKD co-immunoprecipitates with IRS1. *In vivo* constitutively active PKD2 overexpression resulted in a moderate impairment of glucose homeostasis and reduced insulin signaling in the liver. On the contrary, HFD-fed $PKD2^{\Delta Hep}$ male mice displayed improved glucose and pyruvate tolerance, as well as higher peripheral insulin tolerance and enhanced hepatic insulin signaling compared to control $PKD2^{fl/fl}$ mice. Despite of a remodeling of hepatic lipid metabolism in HFD-fed $PKD2^{\Delta Hep}$ mice, similar steatosis grade was found in both genotypes.

Conclusions: Results herein have unveiled an unknown role of PKD2 in the control of insulin signaling in the liver at the level of IRS1 and point PKD2 as a therapeutic target for hepatic insulin resistance.

Keywords Protein kinase D2; Hepatic insulin signaling; Glucose homeostasis; Lipid metabolism

1. INTRODUCTION

The liver plays a fundamental role in regulating glucose homeostasis by maintaining blood glucose within a physiological range [1]. In the fed state, insulin directly and indirectly regulates glucose metabolism by binding to the insulin receptor (IR) in target tissues. Under pathological conditions, impaired hepatic insulin action causes insulin resistance, resulting in the development of type 2 diabetes and its comorbidities including non-alcoholic fatty liver disease (NAFLD) [2], recently renamed as metabolic dysfunction associated steatotic liver disease (MASLD) [3,4].

Protein kinase D (PKD) family of serine/threonine kinases belongs to the Ca^{2+}/Calmodulin-dependent protein kinase (CaMK) superfamily [5]. The mammalian PKD family comprises PKD1, PKD2 and PKD3, encoded by *Prkd1*, *Prkd2* and *Prkd3* (in human *PRKD1*, *PRKD2* and *PRKD3)* genes, respectively [6–9], whose levels and functions vary between tissues

[1]Instituto de Investigaciones Biomédicas Sols-Morreale (IIBM), Consejo Superior de Investigaciones Científicas-Universidad Autónoma de Madrid, Madrid, Spain [2]Centro de Investigación Biomédica en Red de Diabetes y Enfermedades Metabólicas Asociadas (CIBERDEM), Madrid, Spain [3]Department of Physiology, Faculty of Medicine and Nursing, University of the Basque Country UPV/EHU, Leioa, Spain [4]BioBizkaia Health Research Institute, Barakaldo, Spain [5]Centro de Metabolómica y Bioanálisis (CEMBIO), Facultad de Farmacia, Universidad San Pablo-CEU, CEU Universities, Urbanización Montepríncipe, Boadilla del Monte, Spain [6]Liver Research Unit, Santa Cristina University Hospital, Instituto de Investigación Sanitaria Princesa, Madrid, Spain [7]Centro de Investigación Biomédica en Red de Enfermedades Neurodegenerativas (CIBERNED), Madrid, Spain [8]Centro de Investigación Biomédica en Red de Enfermedades Hepáticas y Digestivas (CIBEREHD), Madrid, Spain [9]Centro Nacional de Investigaciones Cardiovasculares Carlos III (CNIC), Madrid, Spain [10]Centro Nacional de Investigaciones Oncológicas (CNIO), Madrid, Spain

[11] Patricia Rada and Elena Carceller-López contributed equally to this work.

[12] Beatriz Gómez-Santos and Constanza Fernández-Hernández contributed equally to this work.

[13] Present address: JP-U, Centro de Biología Molecular "Severo Ochoa" (CSIC-UAM), C/Nicolás Cabrera, 1, 28049 Madrid, Spain.

*Corresponding author. Instituto de Investigaciones Biomédicas Sols-Morreale (CSIC-UAM), Madrid, Spain. E-mail: prada@iib.uam.es (P. Rada).

**Corresponding author. E-mail: avalverde@iib.uam.es (Á.M. Valverde).

Received August 7, 2024 • Revision received September 30, 2024 • Accepted October 7, 2024 • Available online 12 October 2024

https://doi.org/10.1016/j.molmet.2024.102045

Abbreviations

ACC	Acetyl-CoA carboxylase
AKT	Protein Kinase B
ALT	Alanine transaminase
AMPK	AMP-activated protein kinase
BW	Body weight
CHD	Chow diet
DG	Diacylglycerol
EE	Energy expenditure
FA	Fatty acid
FAO	Fatty acid oxidation
FAS	Fatty acid synthase
FOXO1	Forkhead Box O1
GSK3α/β	Glycogen Synthase Kinase 3 α/β
GTT	Glucose tolerance test
HFD	High fat diet
IR	Insulin receptor
IRS1	Insulin receptor substrate 1
ITT	Insulin tolerance test
MASLD	metabolic dysfunction associated steatotic liver disease
NAFLD	Non-alcoholic fatty liver disease
PA	palmitic acid
PKD	Protein Kinase D
PL	Phospholipid
PTT	Pyruvate tolerance test
RER	Respiratory exchange ratio
S6	Ribosomal Protein S6
TG	Triglyceride

[10]. In the last decades, it has become increasingly clear that PKD is at the forefront of the diacylglycerol (DG) signaling network and plays pivotal roles in regulating fundamental biological processes such as signal transduction, membrane trafficking, differentiation, and proliferation [11–13]. In the liver, elevated DGs are attributed to different factors including high fat/high sugar diets and limited expandability of the adipose tissue, leading to an excess of circulating free fatty acids (FAs) [14–16], or elevated oxidative stress [17,18].

Compelling recent evidence supports that PKD family controls glucose homeostasis and insulin sensitivity in a tissue-specific manner. For example, PKD1 hyperactivation in the pancreas increases insulin secretion and protects obese mice against insulin resistance [19]. By contrast, PKD1 depletion in pancreatic beta cells exacerbates high fat diet (HFD)-induced insulin resistance (*i.e.* hyperglycaemia, hyperinsulinemia and glucose intolerance), suggesting PKD1 as a protective candidate against insulin resistance [20]. Also, a recent study [21] showed that mice lacking PKD1 in adipocytes are less insulin resistant and are protected against diet-induced obesity due to beiging in white adipose tissue and increased energy expenditure (EE). Concerning PKD3, its deficiency in hepatocytes increases triglyceride (TG) and cholesterol content in the liver via sterol regulatory element binding protein (SREBP) but, on the other hand, enhances insulin signaling [22]. Related to PKD2, conflicting results have been reported. Whereas global PKD2 deficiency in mice or a loss-of-function mutation in two rhesus monkeys triggers hyperinsulinemia and metabolic disorders [23], its systemic inactivation with a kinase dead mutant ameliorates HFD-induced obesity and type 2 diabetes [24]. Besides, the specific role of PKD2 as a modulator of insulin signaling in hepatocytes and the impact of modulating hepatic PKD2 *in vivo* on insulin sensitivity remain unexplored and are the aims of the present study.

2. MATERIAL AND METHODS

2.1. Reagents

Fetal bovine serum (FBS) and culture media were obtained from ThermoFisher Scientific (Waltham, MA, USA). TRIzol reagent, insulin, palmitic acid (PA) and bovine serum albumin (BSA) were from Sigma Aldrich (St. Louis, MO, USA). Bradford reagent, acrylamide and Clarity ECL Western Blotting Substrate were purchased from Bio-Rad (Hercules, CA, USA). Protein A agarose was purchased from Roche Diagnostics (Indianapolis, IN, USA). CRT0066101 was from Tocris (Bristol, United Kingdom). Methanol (MeOH), acetonitrile (AcN) and isopropanol (IPA), all LC-MS grade, were acquired from Fisher Scientific (Waltham, MA, USA). Ammonium fluoride (NH_4F) (ACS reagent, ≥98%) purchased from Sigma-Aldrich, ammonia solution (28%, GPR RECTAPUR®), and glacial acetic acid (AnalaR®NORMAPUR®) were obtained from VWR Chemicals (Radnor, PN, USA). HPLC grade methyl tert-butyl ether (MTBE) used for lipid extraction was also bought from Sigma-Aldrich. Reverse-osmosed ultrapure water obtained from a Milli-Qplus185 system (Millipore, Billerica, MA, USA). Internal standards (IS) D-erythro-sphinganine (C17 base) bought in Avanti Polar Lipids, Inc., and (R)-3-hydroxypalmitic acid (commercial name d-31 palmitic acid) were purchased from Sigma-Aldrich.

2.2. Animal experimentation

Protocols were approved by the Animal Ethics Committees of CSIC and Comunidad de Madrid in accordance with Spanish (RD53/2013) and European Union (63/2010/EU) legislation (PROEX 246/19). To generate mice with a specific depletion of PKD2 in hepatocytes, B6; 129-*Prkd1*$^{wt/flox}$, *Prkd2*$^{wt/flox}$ mice (provided by A. Harada, Graduate School of Medicine, Osaka University, Suita, Japan) were crossed with C57BL/6J mice to obtain *Prkd1*$^{wt/wt}$-*Prkd2*$^{fl/wt}$ mice (Supplementary Fig. 1a). After producing homozygous B6-*Prkd2*$^{fl/fl}$ mice (PKD2$^{fl/fl}$), they were mated with Alb-Cre$^{+/-}$ mice to generate mice with hepatocyte-specific depletion of PKD2 (PKD2$^{\Delta Hep}$ mice). LoxP sites were inserted in the introns flanking exon 2 in *Prkd2* gene, where one of the two cysteine-rich DG-binding domains is encoded [25,26] (Supplementary Fig. 1b). Cre negative PKD2$^{fl/fl}$ littermates were used as controls. Mice with hepatocyte-specific deletion of PKD1 (PKD1$^{\Delta Hep}$) have been generated using the Cre-LoxP system. Briefly, Alb-Cre$^{+/-}$ mice were intercrossed with mice carrying LoxP-flanked PKD1 (PKD1$^{fl/fl}$ mice) to generate PKD1$^{\Delta Hep}$ mice in a C57BL/6J genetic background (B6-Alb-Cre$^{+/-}$, PKD1$^{fl/fl}$) (Supplementary Fig. 1c). LoxP sites were inserted in the introns flanking exons 12 and 14 in the *Prkd1* gene. Exons 13 and 14 encode the N-terminal region of the kinase domain including the ATP-binding motif [27,28] (Supplementary Fig. 1d). Cre negative PKD1$^{fl/fl}$ littermates were used as controls. C57BL/6J male mice were used when indicated.

Eight-week-old male and female mice were maintained in 12-h light/dark cycle, temperature (22 °C) and humidity-controlled rooms, and fed *ad libitum* a chow diet (CHD, 8.4% (wt/wt) Kcal from fat, (ROD14, Altromin Spezialfutter, Lage, Germany) or a HFD (60% (wt/wt) Kcal from fat, D12492, Research Diets, New Brunswick, NJ, USA) for 14 weeks, with free access to water. Food intake was manually measured and the results are expressed as g/mouse per day and kj/mouse per day. Metabolic tests were conducted in the last 2–4 weeks prior to sacrifice. Four h fasted mice were sacrificed by decapitation. Blood

was collected in tubes coated with ethylenediamine tetraacetic acid (EDTA) to prevent clotting, and immediately centrifuged for 20 min at 15600 × *g* at 4 °C. Plasma was collected, frozen and stored at −80 °C. The liver and skeletal muscle were dissected and snap-frozen. Liver samples were placed in 4 % paraformaldehyde (PFA, 16005, Sigma-Aldrich) for paraffin or optimal cutting temperature (OCT) compound inclusion. Collection of blood for plasma insulin determination is indicated in section 2.7.

2.3. PKD2 overexpression in mouse liver

EGFP-PKD2-CA, a constitutively active human PKD2 fused to EGFP protein where Ser706/Ser710 were mutated to glutamic acid to mimic serine phosphorylation within PKD2 activation loop, was cloned from pEGFP-PKD2-CA-C2 into a hepatocyte-specific human thyroxine binding globulin (TBG) promoter plasmid to generate pAAV[Exp]-TBG > EGFP-PKD2(S706E,S710E)-CA (Vector Builder, Chicago, IL, USA). pAAV[Exp]-CMV > EGFP:WPRE was used as control AAV. AAV plasmids were packaged into AAV-8 capsids to specifically target the liver at the CNIC Viral Vector Unit (Madrid, Spain). Four-week-old C57BL/6J male mice were injected 1×10^{11}adenoviral particles via tail vein, and metabolic tests and insulin signaling analysis were conducted after 10 weeks.

2.4. Indirect calorimetry

Indirect calorimetry analyses were carried out using a 16-chamber TSE PhenoMaster monitoring system (TSE Systems GmbH, Bad Homburg, Germany). Mice were placed in acclimatization cages similar to experimental cages, with one mouse per cage. Acclimation starts 72 h before the beginning of the experiment and the recording was monitored for 5 consecutive days. Mice were on a 12 h light-dark cycle and room temperature was maintained at 22 ± 2 °C. Food and water were provided *ad libitum* in appropriated devices that allow to measure cumulative food intake and drink consumption. Determination of different parameters was carried out over a period of 72 h. RER was estimated by calculating the ratio of VCO_2/VO_2. EE (H(1)) was calculated as: $H(1)\ [kJ \cdot h^{-1} \cdot kg^{-1}] = (3.185 + 1.232 \times RER) \times VO_2 \times 4.184$. Total locomotor activity (ambulatory and fine) was measured simultaneously along the x and y axes using an infrared photocell beam grid, and represented as the average of the total number of beam breaks along the x and y axes during light and dark periods.

2.5. Glucose, insulin, and pyruvate tolerance tests (GTT, ITT, PTT)

For GTT and PTT, 16 h-fasted mice received an intraperitoneal (i.p.) injection of 2 g D-glucose/kg body weight (BW) or 1.5 g sodium pyruvate/kg BW, respectively. For ITT, 4 h-fasted mice received an i.p. injection of 0.75 U insulin/kg BW. Blood glucose was measured with a glucometer (Accu-Check, Roche Diagnostics) before and at 15, 30, 60, 90 and 120 min post-injection, and the area under the curve (AUC) was calculated.

2.6. *In vivo* insulin signaling

Four h-fasted mice were injected 0.75 U/kg BW insulin and sacrificed 15 min later. Blood, liver and skeletal muscle samples were stored at −80 °C.

2.7. Analysis of plasma insulin levels

For insulin determination, plasma was collected from blood obtained from the tail vein with capillary tubes either in fed state or after 24 h fasting. In particular, the blood was centrifuged 20 min at 11600 × *g* at 4 °C; the plasma was then collected and snap-frozen. Plasma insulin levels were measured by ELISA in accordance with the manufacture guidelines (10-1247-01, Mercodia, Uppsala, Sweden).

2.8. Analysis of TG levels in plasma

Plasma TGs levels were measured with a colorimetric kit (11528–11529, Biosystems, Barcelona, Spain) following the manufacturer's instructions.

2.9. Determination of cholesterol levels in plasma

Plasma cholesterol levels were measured using a colorimetric kit (Ref. 1001092, Spinreact, Gerona, Spain) following the manufacturer's instructions.

2.10. Determination of free fatty acids in plasma

Free FA levels were measured using a colorimetric kit (Non-Esterified Fatty Acid (NEFA) Assay Kit, Fujifilm Healthcare solutions, Lexington, MA, USA) following the manufacturer's instructions.

2.11. Analysis of ALT activity in plasma

ALT activity was determined by direct measurement with the Reflotron test (Ref. 10745120, Roche Diagnostics, Basel, Switzerland).

2.12. Histological analysis of liver sections

Hematoxylin and eosin (H&E) staining was performed in paraffin-embedded liver sections. Liver was fixed in 4% (wt/vol) PFA for 24 h, washed twice with phosphate buffered saline (PBS) and dehydrated with ascending ethanol solutions, incubated with xylene and then embedded in paraffin. Blocks were cut in 5 μm sections. Prior to H&E staining, sections were deparaffinized in xylene and hydrated in descending ethanol solutions and distilled water. The slides were stained with Mayer's hematoxylin (MHS32-1L, Sigma-Aldrich) for 15 min and eosin (1.15935.0025, Merck) for 1 min. After dried and mounted, images were captured with an Axiophot light microscope (Zeiss, Oberkochen, Germany) using a 20x objective. Liver biopsies were evaluated by a single blinded hepatopathologist. Steatosis was assessed as outlined by Kleiner et al. [29] grading percentage involvement by steatotic hepatocytes as follows: grade 0, <5 %; grade 1, 5–33 %; grade 2, >33–66 %; and grade 3, >66 %. In addition, this scoring system was used to evaluate the degree of hepatocellular ballooning and lobular inflammation (grade of activity).

2.13. Oil Red O (ORO) staining

Liver sections were fixed overnight with 4% PFA and cryoprotected in subsequent gradients of 15 and 30% sucrose (in PBS) at 4 °C. Afterwards, samples were frozen in Tissue-Tek OCT (Sakura Finetek USA, Torrance, CA, USA) and sectioned at 5 μm using a Leica CM3050 S cryostat. Tissue slides were then left at room temperature for 10 min and the remaining OCT was washed with PBS. Slides were then placed in 60% isopropanol for 15 s before filtering ORO (00625, Merck) solution (60% isoropranol in water) for 15 min. After washing the slides with PBS, they were stained with Carazzi's hematoxylin for 1 min. The excess of the hematoxylin was washed with PBS, after which the slides were mounted in 50% glycerol (in PBS) and sealed. After drying, the images were collected with an Axiophot light microscope (Carl Zeiss).

2.14. Lipidomic studies

2.14.1. Lipid extraction

Approximately 50 mg of liver samples were accurately weighed, transferred to a 2 ml eppendorf tube and thawed in ice to obtain the homogenate. Ten μl of a mixture of MeOH:H_2O 1:1 v/v for each milligram of tissue were added to each tube together with 2 units of 2.8 mm stainless steel balls and the homogenate was obtained by applying 5 cycles of Tissue Lyser QIAGEN® 50 Hz, 5 min each. One

hundred μl of the homogenate was used for the lipid extraction. One hundred μl of cold MeOH with 3 ppm of C17-sphinganine and 6 ppm of d31-palmitic acid were added plus 100 μl of MTBE. Samples were vortexed 1 h at RT and after that, centrifuged for 20 min at 15 °C and 16100 × *g*. Finally, 100 μl of the supernatant was transferred to a chromatography vial (with an insert) twice, one for ESI + ve ionization and the other for ESI −ve ionization analysis. Before direct injection into the UHPLC-QTOF/MS (Agilent 1290 Infinity II UHPLC system), vials were centrifuged for 10 min at 15 °C and 2500 × *g* to avoid bubbles.

2.14.2. UHPLC-QTOF/MS analysis

The lipidomic analysis was performed based on the method previously developed by the CEMBIO group [30]. Randomized samples, for both in ESI + ve and −ve ionization conditions, were directly injected at the Agilent 1290 Infinity II UHPLC system coupled to an Agilent 6545 quadrupole time-of-flight (QTOF) mass spectrometer. This equipment includes an Agilent 1290 Infinity II Multisampler system with a multiwash option, with an injection volume of 1 μl. The multisampler temperature was set at 15 °C to preserve compounds and avoid lipid precipitation. An Agilent InfinityLab Poroshell 120 EC−C18 (3.0 × 100 mm, 2.7 μm) (Agilent Technologies) column and a compatible guard column (Agilent InfinityLab Poroshell 120 EC−C18, 3.0 × 5 mm, 2.7 μm) were used and kept at 50 °C inside the oven. The eluents used in the mobile phase for both ESI +ve and −ve ionization modes contained: (A) 10 mM ammonium acetate and 0.2 mM ammonium fluoride in 9:1 water/methanol; (B) 10 mM ammonium acetate and 0.2 mM ammonium fluoride in 2:3:5 acetonitrile/methanol/isopropanol. The flow rate was established at 0.6 ml/min and keeping constant during the analysis. The elution gradient was from 0 to 1.0 min 70.0% of B and 30.0% of A, to 86.0% of B and 14.0% of A at 3.5−10.0 min, ending with 100.0% of B at 11.0−17.0 min. After that, there was a 2 min re-equilibration time to recover the starting conditions. The total running time was 19.0 min. The multiwash strategy consisted in a mixture of methanol:isopropanol (50:50, v/v) with the wash time set at 15 s, and aqueous phase:organic phase (30:70, v/v) mixture to assist in the starting conditions. The Agilent 6545 QTOF mass spectrometer equipped with a dual AJS ESI ion source was set with the parameters shown in Table 1. Data were collected in ESI + ve and −ve ionization modes in separate runs, in a full scan mode from 50 to 1800 *m/z* with a scan rate of three spectra/s. In addition, a solution consisting of two reference mass compounds was also used during the analysis (Table 1). An Agilent 1260 Iso Pump is capable of infusing into the system these mentioned masses at 1 ml/min (split ratio 1:100) to provide constant mass correction. For both ESI +ve and −ve ionization modes, 10 iterative MS/MS runs were performed, 5 of them with collision energy of 20 eV, and the other 5 at a 40 eV. They were operated with an MS and MS/MS scan rates of 3 spectra/s, 40−1800 *m/z* mass window, a narrow (∼1.3 amu) MS/MS isolation width, 3 precursors per cycle, and 5000 counts and 0.001% of MS/MS threshold.

2.14.3. Data treatment and lipid annotation

Data were collected using MS1 and tandem mass spectrometry (MS2 or MS/MS) from the UHPLC-MS analysis in both ESI positive (+ve) and negative (−ve) ionization modes. MS/MS data were used for accurate lipid annotation with *in silico* databases (Agilent MassHunter Lipid Annotator 1.0) to achieve the most thorough characterization possible using the available bioinformatics and annotation tools. After annotation, data were processed with Agilent MassHunter Profinder B.10.0.2. Following chromatogram alignment, datasets were extracted using the Batch Targeted Feature Extraction workflow with our in-house metabolite library of over 600 manually curated lipids and the list obtained from Lipid Annotator. The algorithm then related the signals to a feature/compound based on retention time, *m/z* (mass/charge), compound mass, and isotopic pattern using MS1 data. Subsequently, data filtering and removal of noise peaks and duplicates were performed. It is important to note that the formation of possible adducts was considered: $[M + H]^+$ and $[M + NH_4]^+$ in ESI positive ionization mode, and $[M-H]^-$ and $[M + CH_3COOH\text{-}H]^-$ in ESI negative ionization mode. Additionally, the option to find features in at least one sample group was selected, considering that we are analyzing two different groups and some features might only appear in one group. Finally, the integration of all peaks was manually reviewed, and annotation was further evaluated based on the MS/MS fragmentation spectra.

2.14.4. Univariate and multivariate analysis

Univariate (UVDA) and multivariate (MVDA) analysis was performed in order to study the possible differences between groups. For both analysis, Metaboanalyst 6.0 online tool was used [31]. Statistical one-factor analysis was carried out. No variance filter, reliability filter or abundance filter was introduced, and also no normalization was introduced in the software. The normalization was done by calculation of relative areas respect to the IS before UVDA and MVDA analysis. Log transformation of the data and pareto scaling was carried out. On one hand, UVDA with Fold Change analysis and *t*-tests were developed. On the other hand, we did MVDA with a first exploratory PCA for a preliminary evaluation of the clustering of the samples and examination of QC grouping. After that, a supervised model Partial Least Squares − Discriminant Analysis (PLS-DA) was built. The quality of the models was assessed by the explained variance (R^2 value) and the predicted variance (Q^2 value), both supplied by the software. Finally, statistically relevant lipids were selected according to VIP score ≥1 (variable importance in VIP projection) (Tables 2 and 3). The two arrays obtained from each ionization mode were treated separately. A total of 82 compounds have been annotated and arranged in different lipid class, together with their corresponding mass, molecular formula, RT (retention time), fold of change comparing $PKD2^{\Delta Hep}$ *versus* $PKD2^{fl/fl}$ mice, *p*-values and VIP score.

2.15. Analysis of hepatic lipid concentration

Pieces of liver tissue (30 mg) were homogenized in PBS and lipids were extracted as described before [32]. TG, DG and phospholipids

Table 1 — Parameters of ESI source and reference masses used in the lipidomic analysis.

Parameters of ESI source		Reference masses	
150 V fragmentor	10 L/min nebulizer gas flow	**Purine** ($C_5H_4N_4$)	*m/z* 121.0509 for the +ve
65 V skimmer	200 °C gas temperature		*m/z* 119.0363 for the -ve
3500 V capillary voltage	50 psi nebulizer gas pressure	**HP-0921** ($C_{18}H_{18}O_6N_3P_3F_{24}$)	*m/z* 922.0098 for the +ve
750 V octopole radio frequency voltage	12 L/min sheath gas flow		*m/z* 980.0163 (+acetate) for the -ve
300 °C sheath gas temperature			

Table 2 — List of relevant features/lipids annotated by this methodology, summarizing all the lipids seen in ESI + ve and -ve ionization modes and in all univariate (UVDA) and multivariate (MVDA) analysis. Each feature is listed with its experimental mass, molecular formula, retention time (min), ionization mode (ESI + ve or -ve) and the corresponding values of Fold Change (FC), p-value (relevant if < 0.05) and VIP score (relevant if ≥ 1) obtained from both statistical analysis.

Compound	Experimental mass	Molecular formula	RT (retention time, min)	ESI ionization mode	FC (Fold Change)	p-value (<0.05)	VIP score (≥1)
Fatty acids							
FA (16:0)	256.2409	$C_{16}H_{32}O_2$	3.5	Negative	0.99	0.022	<1
FA (18:2)	280.2410	$C_{18}H_{32}O_2$	3.1	Negative	1.06	0.293	1.5
FA (18:3)	278.2248	$C_{18}H_{30}O_2$	2.6	Negative	0.70	0.067	1.8
Fatty acyl of hydroxyl fatty acid							
FAHFA (38:6)	582.4630	$C_{38}H_{62}O_4$	3.1	Negative	1.99	0.569	2.1
Carnitines							
CAR (10:0)	315.2368	$C_{17}H_{33}NO_4$	0.9	Positive	0.79	0.064	1.1
Ceramides							
Cer (d40:2)	619.5770	$C_{40}H_{77}NO_3$	11.8	Negative	1.87	0.040	1.8
HexCer (d18:1/22:0)	783.6588	$C_{46}H_{89}NO_8$	11.9	Positive	0.84	0.042	1.0
Diacylglycerols							
DG (16:0_18:3_0:0)	590.4923	$C_{37}H_{66}O_5$	9.5	Negative	1.68	0.031	1.8
DG (16:1_18:1_0:0)	592.5068	$C_{37}H_{68}O_5$	11.3	Positive	2.61	0.055	2.5
DG (16:1_18:2_0:0)	590.4924	$C_{37}H_{66}O_5$	9.5	Negative	1.68	0.034	1.8
DG (32:1)	566.4925	$C_{35}H_{66}O_5$	11.0	Positive	1.68	0.032	2.0
DG (34:1)	594.5239	$C_{37}H_{70}O_5$	11.8	Positive	1.72	0.017	2.0
				Negative	1.71	0.039	1.8
DG (34:2)	592.5077	$C_{37}H_{68}O_5$	11.3	Negative	1.67	0.030	1.7
Phosphatidylcholines							
PC (0:0/20:3)	545.3479	$C_{28}H_{52}NO_7P$	2.2	Positive	1.38	0.034	1.4
PC (0:0/20:4)	543.3341	$C_{28}H_{50}NO_7P$	1.9	Positive	1.39	0.017	1.4
PC (14:0_18:2)	729.5301	$C_{40}H_{76}NO_8P$	6.2	Positive	0.78	0.023	1.3
PC (16:0/18:2)	757.5639	$C_{42}H_{80}NO_8P$	7.7	Positive	0.81	0.021	1.2
PC (16:0/18:3)	755.5466	$C_{42}H_{78}NO_8P$	6.8	Positive	0.66	0.034	1.7
				Negative	0.63	0.039	1.3
PC (16:0/22:5)	807.5743	$C_{46}H_{82}NO_8P$	8.9	Positive	0.84	0.050	1.0
PC (18:0/16:0)	761.5951	$C_{42}H_{84}NO_8P$	11.1	Positive	0.84	0.020	1.1
PC (16:1_18:2)	755.5467	$C_{42}H_{78}NO_8P$	6.8	Negative	0.63	0.039	1.3
PC (18:0/16:3)	755.5464	$C_{42}H_{78}NO_8P$	7.0	Positive	0.68	0.040	1.6
				Negative	0.63	0.039	1.3
PC (18:0/20:1)	815.6397	$C_{46}H_{90}NO_8P$	11.8	Positive	0.72	0.002	1.7
PC (18:0_18:3)	783.5746	$C_{44}H_{82}NO_8P$	11.1	Positive	0.86	0.005	1.0
PC (18:1/20:1)	813.6261	$C_{46}H_{88}NO_8P$	11.5	Positive	0.67	0.007	1.7
				Negative	0.57	0.047	1.3
PC (18:1_20:4)	807.5793	$C_{46}H_{82}NO_8P$	8.1	Positive	0.53	0.049	1.7
PC (18:2/18:2)	781.5620	$C_{44}H_{80}NO_8P$	7.4	Positive	0.71	0.015	1.6
PC (19:0_18:2)	799.6050	$C_{45}H_{86}NO_8P$	10.9	Positive	0.60	0.012	1.9
				Negative	0.70	0.044	1.0
PC (20:0_20:2)	841.6594	$C_{48}H_{92}NO_8P$	11.9	Positive	0.72	0.001	1.7
				Negative	0.70	0.039	1.0
PC (33:3)	741.5309	$C_{41}H_{76}NO_8P$	8.2	Positive	0.56	0.000	2.4
				Negative	0.56	0.004	1.6
PC (39:6)	819.5796	$C_{47}H_{82}NO_8P$	7.9	Positive	0.72	0.049	1.4
PC (40:3)	839.6419	$C_{48}H_{90}NO_8P$	11.7	Positive	0.73	0.007	1.5
PC (40:5)	835.6068	$C_{48}H_{86}NO_8P$	11.5	Positive	0.70	0.001	1.8
PC (42:4)	865.6552	$C_{50}H_{92}NO_8P$	11.9	Positive	0.67	0.002	1.8
PC (42:5)	863.6375	$C_{50}H_{90}NO_8P$	11.5	Positive	0.71	0.028	1.5
PC (O-18:0/20:4)	795.6148	$C_{46}H_{86}NO_7P$	10.9	Positive	0.68	0.080	1.4
PCO-32:1/PCP-32:0	717.5657	$C_{40}H_{80}NO_7P$	8.6	Positive	0.71	0.020	1.6
PCO-33:6/PCP-33:5	721.5040	$C_{41}H_{72}NO_7P$	7.7	Positive	0.78	0.031	1.3
PCO-35:4/PCP 35:3	753.5665	$C_{43}H_{80}NO_7P$	11.3	Positive	0.70	0.055	1.5
PCO-37:1/PCP-37:0	787.6467	$C_{45}H_{90}NO_7P$	11.6	Positive	0.61	0.004	2.0
PCO-37:10/PCP-37:9	769.5050	$C_{45}H_{72}NO_7P$	7.5	Positive	0.30	0.184	2.1
PCO-38:4/PCP-38:3	795.6149	$C_{46}H_{86}NO_7P$	10.9	Positive	0.68	0.080	1.4
PCO-39:10/PCP-39:9	797.5360	$C_{47}H_{76}NO_7P$	9.0	Positive	0.69	0.004	<1
PCO-39:7/PCP-39:6	803.5823	$C_{47}H_{82}NO_7P$	11.7	Positive	0.67	0.020	1.6
PCO-39:8/PCP-39:7	801.5691	$C_{47}H_{80}NO_7P$	11.7	Positive	0.69	0.022	1.6
PCO-41:11/PCP-41:10	823.5522	$C_{49}H_{78}NO_7P$	9.6	Positive	0.67	0.022	1.6
PCO-42:7/PCP-42:6	845.6292	$C_{50}H_{88}NO_7P$	11.6	Positive	0.60	0.035	1.8
Phosphatidylethanolamines							
PE (0:0/18:2)	477.2869	$C_{23}H_{44}NO_7P$	2.0	Positive	0.71	0.024	1.5
				Negative	0.68	0.005	1.2
PE (16:0/18:2)	715.5128	$C_{39}H_{74}NO_8P$	7.9	Positive	0.57	0.011	2.1
				Negative	0.52	0.007	1.5

(*continued on next page*)

Table 2 — (*continued*)

PE (16:0/20:4)	739.5166	C_{41} H_{74} N O_8 P	7.7	Positive	0.77	0.032	1.3
PE (16:0/22:5)	765.5304	C_{43} H_{76} N O_8 P	8.5	Positive	0.43	0.105	1.9
PE (16:0/22:6)	763.5176	C_{43} H_{74} N O_8 P	7.4	Positive	0.77	0.045	1.3
PE (18:0/18:1)	745.5602	C_{41} H_{80} N O_8 P	11.5	Positive	0.71	0.051	1.4
PE (18:0/18:2)	743.5467	C_{41} H_{78} N O_8 P	9.9	Negative	0.55	0.001	1.7
PE (18:0/20:3)	769.5608	C_{43} H_{80} N O_8 P	10.9	Positive	0.71	0.001	1.7
PE (18:0/22:4)	795.5778	C_{45} H_{82} N O_8 P	11.6	Positive	0.58	0.014	2.0
				Negative	0.53	0.024	1.5
PE (18:0/22:5)	793.5602	C_{45} H_{80} N O_8 P	10.9	Positive	0.40	0.126	1.8
PE (18:1/18:2)	741.5309	C_{41} H_{76} N O_8 P	8.2	Positive	0.56	0.000	2.4
				Negative	0.56	0.004	1.6
PE (18:1/20:4)	765.5311	C_{43} H_{76} N O_8 P	8.0	Positive	0.77	0.029	1.3
PE (O-18:0_20:4)	753.5664	C_{43} H_{80} N O_7 P	11.3	Positive	0.70	0.053	1.5
PE (0—18:1_20:3)/PE (P-18:0_20:3)	753.5665	C_{43} H_{80} N O_7 P	11.3	Positive	0.71	0.055	1.4
PE (O-18:1/20:4)/PE (P-18:0/20:4)	751.5515	C_{43} H_{78} N O_7 P	11.1	Positive	0.70	0.026	1.6
				Negative	0.70	0.032	1.0
PE (O-20:1_22:5)/PE (P-20:0_22:5)	773.5348	C_{45} H_{76} N O_7 P	11.1	Positive	0.71	0.024	1.5
PE (40:9)	785.4978	C_{45} H_{72} N O_8 P	7.4	Positive	0.79	0.048	1.2
PEO-42:7/PEP-42:6	803.5777	C_{47} H_{82} N O_7 P	11.7	Positive	0.73	0.026	1.5
				Negative	0.52	0.026	1.6
Phosphatidylinositol							
PI (16:0/18:1)	836.5399	C_{43} H_{81} O_{13} P	6.9	Positive	0.80	0.023	1.2
PI (16:0/18:2)	834.5265	C_{43} H_{79} O_{13} P	6.0	Positive	0.72	0.012	1.5
				Negative	0.56	0.015	1.5
PI (16:0/20:3)	860.5385	C_{45} H_{81} O_{13} P	6.1	Positive	0.84	0.030	1.1
PI (16:0/20:4)	858.5234	C_{45} H_{79} O_{13} P	5.9	Positive	0.73	0.029	1.5
PI (18:0/18:2)	862.5578	C_{45} H_{83} O_{13} P	7.1	Negative	0.62	0.034	1.2
PI (18:0/20:4)	886.5584	C_{47} H_{83} O_{13} P	7.0	Positive	0.86	0.008	1.1
PI (18:1/18:1)	862.5578	C_{45} H_{83} O_{13} P	7.1	Negative	0.62	0.034	1.2
Phosphatidylserines							
PS (40:6)	835.5350	C_{46} H_{78} N O_{10} P	6.9	Positive	0.74	0.024	1.4
Sphingomyelin							
SM(d-18:0/16:0)	704.5826	C_{39} H_{81} N_2 O_6 P	7.6	Positive	0.74	0.055	1.3
SM (d18:0/24:1)	814.6932	C_{47} H_{95} N_2 O_6 P	12.1	Positive	0.68	0.012	1.7
SM (d18:1/14:0)	674.5356	C_{37} H_{75} N_2 O_6 P	5.7	Negative	0.66	0.028	<1
SM (d18:1/15:0)	688.5510	C_{38} H_{77} N_2 O_6 P	6.3	Positive	0.82	0.041	1.1
SM (d18:1/17:0)	716.5839	C_{40} H_{81} N_2 O_6 P	7.7	Positive	0.74	0.036	1.4
SM (d18:1/23:0)	800.6750	C_{46} H_{93} N_2 O_6 P	12.0	Positive	0.75	0.050	1.3
SM (d18:1/24:0)	814.6932	C_{47} H_{95} N_2 O_6 P	12.1	Positive	0.68	0.011	1.7
				Negative	0.66	0.027	1.1
SM (d18:2/23:0)/SM(d19:1/22:1)	798.6601	C_{46} H_{91} N_2 O_6 P	11.6	Positive	0.70	0.027	1.5
SM (d19:1/16:0)	716.5829	C_{40} H_{81} N_2 O_6 P	7.7	Positive	0.73	0.037	1.4
SM (d19:1/22:1)/SM(d18:2/23:0)	798.6601	C_{46} H_{91} N_2 O_6 P	11.6	Positive	0.71	0.026	1.5
SM (d18:2/22:0)	784.6414	C_{45} H_{89} N_2 O_6 P	11.3	Negative	0.63	0.034	1.3

(PLs) were separated by thin layer chromatography (TLC) as described previously [33]. TLC plates were scanned using a ChemiDoc image acquirer and band corresponding to TG, DG and PLs were quantified using Image Lab software (BioRad) as detailed in [34].

2.16. Measurement of fatty acid oxidation (FAO) rate

The FAO rate was assessed as described before [35]. Briefly, 30 mg of freshly isolated liver pieces were homogenized in cold homogenization STE buffer (25 mM Tris-HCl, 500 nM sucrose, 1 mM EDTA-Na_2 pH 7.4) and sonicated for 10 s. Then, the homogenates were centrifuged at 420 $\times$ *g* for 10 min at 4 °C and the supernatant was collected. 500 μg of protein from the liver homogenates were used for the assay in a volume of 60 μl. The reaction started by adding 340 μl of assay buffer containing 0.5 μCi/ml [1—^{14}C]-Palmitic acid to the samples. Samples were incubated for 30 min at 37 °C in eppendorf tubes with a Whatman paper circle in the cap. The reaction was stopped by adding 200 μl of 3 M perchloric acid, after adding 1 M NaOH in the Whatman cap to collect all the evaporated [^{14}C]-CO_2. After 1 h, the Whatman caps were removed and the associated radioactivity was measured in a scintillation counter.

2.17. Measurement of *de novo* lipogenesis

De novo lipogenesis was performed as previously described [36] with slight modifications. In brief, freshly isolated tissue slices (around 40 mg) were incubated in high glucose DMEM with insulin (150 nM) and [H^3] acetic acid 20 μCi/ml for 4 h. Tissue slices were washed five times in cold PBS, homogenized in PBS and lipids were extracted as previously described [32]. Then, lipids were separated by TLC [33], each lipid was scraped and the radioactivity was measured in a scintillation counter.

2.18. Homogenization and preparation of tissue extracts

Frozen liver tissues were homogenized in ice-cold lysis buffer containing 50 mM Tris-HCl, 1% (vol/vol) Triton X-100, 2 mM EGTA, 10 mM EDTA acid, 100 mM NaF, 1 mM $Na_4P_2O_7$, 2 mM Na_3VO_4, 100 μg/ml phenylmethylsulphonyl fluoride (PMSF), 2.5 μg/ml protease inhibitors (P8340, ThermoFisher Scientific) and PhosSTOP inhibitor tablet (Sigma-Aldrich) by using the Brinkman PT 10/35 Polytron. Extracts were always kept ice-cold. Tissue extracts were cleared twice by ultracentrifugation at 40000 $\times$ *g* for 40 min at 4 °C. Protein

Table 3 — List of Triglycerides annotated by this methodology, summarizing all the TGs seen in ESI + ve and -ve ionization modes and in all univariate (UVDA) and multivariate (MVDA) analysis. Each feature is listed with its experimental mass, molecular formula, retention time (min), ionization mode (ESI + ve or -ve) and the corresponding values of Fold Change (FC), p-value (relevant if < 0.05) and VIP score (relevant if ≥ 1) obtained from both statistical analysis.

Compound	Experimental mass	Molecular formula	RT (retention time, min)	ESI ionization mode	FC (Fold Change)	p-value (<0.05)	VIP score (≥1)
Triglycerides							
TG (10:0_18:1_18:2)	772.6573	$C_{49}H_{88}O_6$	12.9	Positive	0.78	0.059	1.2
TG (12:0_18:2_18:2)	798.6731	$C_{51}H_{90}O_6$	12.9	Positive	0.81	0.120	<1
TG (14:2_18:2_18:2)	822.6721	$C_{53}H_{90}O_6$	13.1	Positive	0.98	0.862	<1
TG (16:0_18:1_22:6)	904.7511	$C_{59}H_{100}O_6$	13.3	Positive	0.79	0.392	<1
TG (18:0_18:1_22:6)	932.7812	$C_{61}H_{104}O_6$	14.4	Positive	0.86	0.481	<1
TG (18:1_18:1_20:0)	914.8306	$C_{59}H_{110}O_6$	15.7	Positive	0.89	0.419	<1
TG (18:1_18:1_22:2)	938.8299	$C_{61}H_{110}O_6$	14.9	Positive	0.76	0.219	<1
TG (18:1_18:3_18:1)	928.7477	$C_{61}H_{100}O_6$	13.7	Positive	0.85	0.410	<1
TG (18:2_18:2_18:3)	876.7206	$C_{57}H_{96}O_6$	13.2	Positive	0.97	0.919	<1
TG (18:2_18:2_20:5)	900.7194	$C_{59}H_{96}O_6$	12.9	Positive	0.90	0.748	<1
TG (18:2_20:3_20:0)	936.8124	$C_{61}H_{108}O_6$	14.5	Positive	0.73	0.352	<1
TG (18:3_20:3_20:5)	924.7210	$C_{61}H_{96}O_6$	13.2	Positive	0.90	0.768	<1
TG (22:5_18:1_18:1)	932.7836	$C_{61}H_{104}O_6$	13.9	Positive	0.47	0.192	1.5
TG (46:1)	776.6895	$C_{49}H_{92}O_6$	13.5	Positive	1.02	0.738	<1
TG (46:2)	774.6720	$C_{49}H_{90}O_6$	13.1	Positive	0.93	0.114	<1
TG (48:0)	806.7360	$C_{51}H_{98}O_6$	14.4	Positive	0.95	0.186	<1
TG (48:1)	804.7212	$C_{51}H_{96}O_6$	13.9	Positive	1.17	0.339	<1
TG (48:2)	802.7057	$C_{51}H_{94}O_6$	13.5	Positive	1.13	0.491	<1
TG (48:3)	800.6897	$C_{51}H_{92}O_6$	13.1	Positive	0.98	0.843	<1
TG (49:2)	816.7202	$C_{52}H_{96}O_6$	13.7	Positive	1.05	0.501	<1
TG (49:3)	814.7050	$C_{52}H_{94}O_6$	13.3	Positive	0.95	0.166	<1
TG (50:1)	832.7532	$C_{53}H_{100}O_6$	14.4	Positive	1.18	0.282	<1
TG (50:2)	830.7379	$C_{53}H_{98}O6$	13.9	Positive	1.18	0.352	<1
TG (50:3)	828.7218	$C_{53}H_{96}O_6$	13.5	Positive	1.18	0.352	<1
TG (50:4)	826.7053	$C_{53}H_{94}O_6$	13.2	Positive	1.07	0.605	<1
TG (51:2)	844.7517	$C_{54}H_{100}O_6$	14.1	Positive	1.11	0.419	<1
TG (51:3)	842.7362	$C_{54}H_{98}O_6$	13.7	Positive	1.02	0.857	<1
TG (52:1)	860.7836	$C_{55}H_{104}O_6$	15.0	Positive	1.07	0.698	<1
TG (52:2)	858.7697	$C_{55}H_{102}O_6$	14.4	Positive	1.17	0.365	<1
TG (52:3)	856.754	$C_{55}H_{100}O_6$	13.9	Positive	1.05	0.774	<1
TG (52:4)	854.7378	$C_{55}H_{98}O_6$	13.5	Positive	0.95	0.808	<1
TG (52:5)	852.7194	$C_{55}H_{96}O_6$	13.3	Positive	0.90	0.652	<1
TG (52:6)	850.7029	$C_{55}H_{94}O_6$	13.5	Positive	1.17	0.327	<1
TG (53:6)	864.7176	$C_{56}H_{96}O_6$	13.7	Positive	1.04	0.705	<1
TG (54:2)	886.7996	$C_{57}H_{106}O_6$	14.9	Positive	1.08	0.650	<1
TG (54:3)	884.7852	$C_{57}H_{104}O_6$	14.4	Positive	1.09	0.658	<1
TG (54:4)	882.7694	$C_{57}H_{102}O_6$	13.9	Positive	0.97	0.825	<1
TG (54:5)	880.7531	$C_{57}H_{100}O_6$	13.7	Positive	0.97	0.833	<1
TG (54:6)	878.7375	$C_{57}H_{98}O_6$	13.4	Positive	0.91	0.713	<1
TG (54:7)	876.7208	$C_{57}H_{96}O_6$	13.5	Positive	0.96	0.815	<1
TG (54:8)	874.7014	$C_{57}H_{94}O_6$	13.3	Positive	0.91	0.645	<1
TG (56:10)	926.7315	$C_{61}H_{98}O_6$	13.1	Positive	0.90	0.747	<1
TG (56:3)	912.8152	$C_{59}H_{108}O_6$	14.9	Positive	0.96	0.860	<1
TG (56:4)	910.7992	$C_{59}H_{106}O_6$	14.4	Positive	0.87	0.558	<1
TG (56:5)	908.7807	$C_{59}H_{104}O_6$	14.1	Positive	0.90	0.577	<1
TG (56:6)	906.7683	$C_{59}H_{102}O_6$	13.7	Positive	0.91	0.686	<1
TG (56:7)	904.7514	$C_{59}H_{100}O_6$	13.4	Positive	0.78	0.346	<1
TG (56:8)	902.7329	$C_{59}H_{98}O_6$	13.6	Positive	0.84	0.241	<1
TG (58:6)	934.7997	$C_{61}H_{106}O_6$	14.1	Positive	0.68	0.372	<1
TG (58:8)	930.7637	$C_{61}H_{102}O_6$	14.1	Positive	0.90	0.574	<1

concentration was determined by using the Pierce BCA Protein Assay Kit (23227, ThermoFisher Scientific).

Muscle extracts were prepared in cold lysis buffer containing 50 mM Tris-HCl pH 7.5, 1 mM EGTA, 1 mM EDTA, 50 mM NaF, 1 mM sodium β-glycerophosphate, 5 mM sodium pyrophosphate, 0.27 M sucrose, 1% (vol/vol) Triton X-100, 0.1% (vol/vol) β-mercaptoethanol, 1 mM Na_3VO_4, 100 μg/ml PMSF and 2.5 μg/ml protease inhibitors by using the Brinkman PT 10/35 Polytron. Lysates were centrifuged at 19000 × *g* for 20 min at 4 °C and protein content of the supernatants was determined by the Bradford method (5000006, Bio-Rad Laboratories).

2.19. Primary culture of mouse hepatocytes

Primary mouse hepatocytes were isolated from non-fasting male mice by a two-step perfusion with collagenase [37]. Cells were seeded on collagen IV pre-coated plates (Corning, New York, NY, USA), cultured in DMEM-Ham's F-12 medium (1:1) with heat-inactivated 10% (vol/vol) FBS supplemented with 2 mM glutamine, 15 mM glucose, 20 mM HEPES, 100 U/ml penicillin, 100 μg/ml streptomycin and 1 mM sodium pyruvate, and maintained for 24 h at 37 °C in a humidified atmosphere with 5% CO_2. Then, medium was replaced to serum-free DMEM supplemented with 5.5 mM glucose 2 h prior to insulin stimulation. To inhibit PKDs, CRT0066101 was

added at the same time as the medium was replaced. After 2 h, hepatocytes were stimulated with insulin.

2.20. Silencing of *Prkd1* and *Prkd2* in primary mouse hepatocytes by siRNA transfection

siRNA oligos were synthesized by Dharmacon RNAi Technologies for gene silencing of mouse *Prkd1* and *Prkd2*. Primary mouse hepatocytes were seeded in 6 cm dishes and incubated at 37 °C with 5% CO_2 overnight. The following day cells were transfected with siRNA for *Prkd1* or *Prkd2,* respectively, or with a scramble siRNA at 25 nM concentration following DharmaFECT General Transfection Protocol (Dharmacon, Lafayette, CO, USA). After 36 h, medium was replaced to serum-free DMEM supplemented with 5.5 mM glucose for 2 h and then, cells were stimulated with insulin.

2.21. Culture of human and mouse hepatic cell lines

Huh6 and Huh7 human hepatocarcinoma cells, free of mycoplasma, were cultured in DMEM supplemented with 10% (vol/vol) heat-inactivated FBS, 100 U/ml penicillin and 100 μg/ml streptomycin. Generation of immortalized mouse hepatocytes was previously described [38]. For experiments, culture medium was replaced to serum-free DMEM supplemented with 5.5 mM glucose 2 h prior to insulin stimulation.

2.22. Lentiviral silencing of *Prkd2* in immortalized mouse hepatocytes

Lentiviral suspensions were prepared in HEK293T cells as follows: HEK293T were transfected with lentiviral vectors containing either *Prkd2* shRNA (MISSION pLKO.1-puro-*Prkd2* shRNA Plasmid DNA, Sigma-Aldrich) or control shRNA (MISSION pLKO.1-puro Empty Vector Control Plasmid DNA, Sigma-Aldrich) and packaging vectors (psPAX2 and pMD2.G plasmids) using PEI reagent (Polyethylenimine, Linear, MW 25000, Transfection Grade, Polysciences Inc. Warrington, PA, USA) and OPTIMEM media (ThermoFisher Scientific) for 24 h. Medium was then changed to DMEM supplemented with 10% (vol/vol) heat-inactivated FBS, penicillin (100 U/ml), and streptomycin (100 U/ml). Supernatants were collected after 24 h. Immortalized mouse hepatocytes were transduced with these supernatants containing lentiviral particles bearing shRNA for *Prkd2* (sh*Prkd2*). Control shRNA lentiviral particles were used as a control (shControl). In parallel and to test the transduction efficiency, hepatocytes were infected with lentiviral particles bearing EGFP (pWPXL-EGFP). After 5 days, culture medium was replaced to serum-free DMEM supplemented with 5.5 mM glucose 1 h prior to insulin stimulation. Gene knockdown was confirmed by measuring pPKD1/2 protein levels.

2.23. EGFP-PKD2-CA overexpression in Huh7 cells

Huh7 cells were transfected with pEGFP-C2 empty vector or containing a constitutively active version of PKD2 (EGFP-PKD2-CA) using 0.5 μg of DNA and 5 μl of Lipofectamine 2000 reagent (ThermoFisher Scientific, Waltham, MA, USA) per well, according to the manufacturer's specifications. EGFP-PKD2-CA is a constitutively active human PKD2 mutant, where Ser706 and Ser710 residues were mutated to glutamic acid to mimic serine phosphorylation within the activation loop of PKD2. Medium was changed at 8 h post-transfection. After 16 h, cells were serum-starved for a further 2 h and then stimulated with insulin.

2.24. Co-immunoprecipitation assays

Cells were scraped off in lysis buffer containing 10 mM Tris-HCl, 5 mM EDTA, 50 mM NaCl, 30 mM disodium pyrophosphate, 50 mM NaF, 100 μM Na_3VO_4, 1% (vol/vol) Triton X-100, 1 mM PMSF and 2.5 μg/ml protease inhibitors (pH 7.6). Cellular lysates were clarified by centrifugation at 12000 × *g* for 10 min. Protein content was determined by the Bradford method (5000006, Bio-Rad Laboratories), and equal amount of proteins (500 μg) were immunoprecipitated at 4 °C with the anti-IRS1 or anti-PKD2 antibodies (Table 4). Immune complexes were collected on Protein A-Agarose beads (Roche, Basel, Switzerland) and subjected to Western blot analysis.

2.25. Preparation of protein lysates from hepatic cells

After culture and treatments, cells were washed twice with PBS, then scraped off in the lysis buffer described in the co-immunoprecipitation assays. Cellular lysates were clarified by centrifugation at 12000 × *g* for 10 min. Protein content was determined by the Bradford method (5000006, Bio-Rad Laboratories).

2.26. Western blot analysis

Protein extracts either from hepatic cells or from tissue were boiled at 95 °C for 5 min in loading buffer (100 mM Tris, pH 6.8, 10% (vol/vol) glycerol, 4% (wt/vol) sodium dodecyl sulphate (SDS), 0.2% (wt/vol) bromophenol blue, and 2 mM β-mercaptoethanol), subjected to SDS polyacrylamide gel electrophoresis (SDS-PAGE), and then transferred to PVDF membranes (Immobilon-P IPVH00010, Merck, Darmstadt, Germany). Membranes were blocked with 5% non-fat dry milk or 4% BSA in TBS supplemented with 0.05% (vol/vol) Tween-20 (TTBS) for 2 h at RT and then, incubated with primary antibodies as indicated in TTBS overnight at 4 °C. After 3 washes with TTBS, membranes were incubated with the corresponding peroxidase-conjugated secondary antibodies (anti-rabbit, 1/15000, A120-108P, Bethyl Laboratories (Montgomery, TX, USA); anti-mouse, 1/10000, sc-2005, Santa Cruz Biotechnology, Dallas, TX, USA)) for 1 h at RT. Membranes were developed with chemiluminescent substrate (Clarity Western ECL Substrate, 170−5060, Bio-Rad Laboratories) and different exposure times were performed for each primary antibody with radiographic films in a radiology cassette (AGFA, Mortsel, Belgium) or developed in a ChemiDoc imager (Bio-Rad Laboratories). Primary antibodies used were listed in Table 4. Blots were normalized using antibodies against housekeeping proteins. Densitometry values were determined using Fiji Software [39] or Image Lab Software (Bio-Rad Laboratories).

2.27. Quantitative real-time PCR (RT-qPCR) analysis

Total RNA was extracted with TRIzol reagent from hepatic cells or liver tissue and reverse transcribed using a SuperScript III First-Strand Synthesis System for qRT-PCR following the manufacturer's indications (ThermoFisher Scientific). qRT-PCR was performed with an 7900HT Fast Real-Time PCR System. Primer sequences were described in Table 5. Data analysis is based on the ΔΔCt method with normalization of the raw data to housekeeping genes as described in the manufacturer's manual (Applied Biosystems).

2.28. Data analysis

For animal experiments, sample size was chosen based on similar previous studies of our group and on the basis of literature documentation of similar well-characterized experiments [40−43]. The fewest number of mice were used to achieve statistical significance. Statistical analysis was performed using the GraphPad Prism software version-8.0 (San Diego, CA, USA). Data are reported as mean and standard error of the mean (SEM). Grubbs's or ROUT tests were used to identify outliers. Normal distribution was assessed by Shapiro-Wilk and Kolmogorov-Smirnov tests. For data with parametric distributions, unpaired Student's t test was used to compare mean differences between two groups, and for three or more groups, one-way ANOVA with Bonferroni

Table 4 — List of used primary antibodies.

Antibody	Manufacturer	Catalogue number	Host species	Dilution for WB
Phospho-ACC Ser79	Cell Signaling Technology	3661	Rabbit	1:2000
ACC	Cell Signaling Technology	3662	Rabbit	1:2000
Phospho-AKT Ser 473	Cell Signaling Technology	4058	Rabbit	1:2000
Phospho-AKT Thr308	Cell Signaling Technology	4056	Rabbit	1:1000
AKT	Cell Signaling Technology	4691	Rabbit	1:20000
Phospho-AMPKα Thr172	Cell Signaling Technology	2531	Rabbit	1:2000
AMPKα	Cell Signaling Technology	2532	Rabbit	1:1000
EGFP	Roche	11814460001	Mouse	1:2000
Phospho-p44/42 MAPK (ERK1/2) (Thr202/Tyr204)	Cell Signaling Technology	9101	Rabbit	1:2000
p44/42 MAPK (ERK1/2) (137F5)	Cell Signaling Technology	4695	Rabbit	1:3000
Phospho-FOXO1 Ser256	Cell Signaling Technology	9461	Rabbit	1:1000
FOXO1	Cell Signaling Technology	9454	Rabbit	1:1000
Phospho-GSK-3α/β Ser21/9	Cell Signaling Technology	8566	Rabbit	1:1000
GSK-3α/β	Santa Cruz Biotechnology	sc-7291	Mouse	1:2000
Phospho-IKKα (Ser180)/IKKβ (Ser181)	Cell Signaling Technology	2681	Rabbit	1:1000
IKKα/β (H-470)	Santa Cruz Biotechnology	sc-7607	Rabbit	1:1000
Phospho-IRβ	Cell Signaling Technology	3024	Rabbit	1:1000
IRβ	Cell Signaling Technology	3025	Rabbit	1:2000
Phospho-IRS1 Tyr608 (mouse)/Tyr612 (human)	Merck Millipore	09—432	Rabbit	1:5000
Phospho-IRS1 Ser612 (mouse)/Ser616 (human)	Cell Signaling Technology	3203	Rabbit	1:1000
IRS1	Merck Millipore	06—428	Rabbit	1:2000
Phospho-SAPK/JNK (Thr183/Tyr185)	Cell Signaling Technology	9251	Rabbit	1:1000
JNK (FL)	Santa Cruz Biotechnology	sc-571	Rabbit	1:2000
Phospho-PKD1/2 Ser 916/Ser873	Cell Signaling Technology	2051S	Rabbit	1:1000
Phospho-PKD2 Ser873	Sigma-Aldrich	SAB4504104	Rabbit	1:1000
Mouse PKD1/2	Cell Signaling Technology	2052S	Rabbit	1:1000
Human PKD2	Cell Signaling Technology	8188S	Rabbit	1:2000
Phospho-S6 Ribosomal Protein Ser235	Cell Signaling Technology	2211	Rabbit	1:1000
S6 Ribosomal Protein	Cell Signaling Technology	2217	Rabbit	1:4000
Phospho-Ser clone 4A4	Merck Millipore	05-1000X	Rabbit	1:1000
GAPDH	Abcam	ab8245	Mouse	1:5000
α-Tubulin	Sigma-Aldrich	T5168	Mouse	1:5000
Vinculin	Santa Cruz Biotechnology	sc-7314	Mouse	1:7500

post hoc test was used. For data with non-parametric distributions, differences between groups were examined with Mann-Whitney U test for two groups. Two-way ANOVA with Bonferroni *post hoc* test was employed to compare two different categorical, independent variables. The sample size and the power to detect the differences between experimental groups are provided in Figure Legends. Tests were two-sided and $p < 0.05$ was considered statistically significant.

3. RESULTS

3.1. PKD2 inhibition enhances insulin-induced AKT phosphorylation in hepatocytes

As an initial approach to decipher the impact of global PKD inhibition in the regulation of insulin signaling in hepatocytes, primary mouse hepatocytes were treated with CRT0066101, a pan-PKD inhibitor [44,45]. As expected, CRT0066101 (2.5—10 μM) diminished the catalytic activity of PKD1/2, as reflected by a reduction in PKD1/2 autophosphorylation at Ser916 and Ser873 residues (Supplementary Fig. 2a). Pretreatment with CRT0066101 2 h prior to insulin stimulation (10 nM, 5 min) dose-dependently enhanced insulin signaling by elevating phospho-protein kinase B (AKT) (Ser473 and Thr308) levels (Supplementary Fig. 2a). Similar results were observed when PKDs were inhibited in Huh7 and Huh6 human hepatocytes (Supplementary Fig. 2b, c). Since on the one hand PKD3 suppreses the activity of insulin signaling effectors [22] and, on the other, the mRNA levels of PKD1 are very low in primary mouse hepatocytes (Figure 1A), herein we aimed to investigate the contribution of PKD2 isoform to the modulation of insulin signaling. We first silenced *Prkd2* in primary

Table 5 — List of primers and Taqman probes used in qRT-PCR assays.

Gene	Forward primer	Reverse primer
Prkd1	5′- CCGGATCCAACTCACACAAAGA-3′	5′- CAAACTGTCCGGAACCCAGA-3′
Prkd2	5′- CTTGGATCTCCAGTCGCCG -3′	5′- ACATGAGCCAACTCTGAGGC-3′
Prkd3	5′-AAGAGACATTATTGGAGACTTGGACAG-3′	5′-AGTGTGGGTTACTGCCTTGTG-3′
G6pc	5′-TCCCCAGAATTCTCCACTTG-3′	5′-AACATCGGAGTGACCTTTGG-3′
Pck1	5′-AAGCATTCAACGCCAGGTTC-3′	5′-GGGCGAGTCTGTCAGTTCAAT-3′
Gapdh	5′-AGGTCGGTGTGAACGGATTTG-3′	5′- TGTAGACCATGTAGTTGAGGTCA-3′
Actb	5′-AGGAGGAGCAATGATCTTGATCTT-3′	5′- TCCTTCCTGGGCATGGAG-3′
Rplp0	5′-ACTGGTCTAGGACCCGAGAAG-3′	5′TCCCACCTTGTCTCCAGTCT-3′
Gene	**Taqman probes**	
Prkd1	Mm01284193_m1/Mm00435792_m1	
Prkd2	Mm00626821_m1	
Rplp0	Mm01974474_gH	

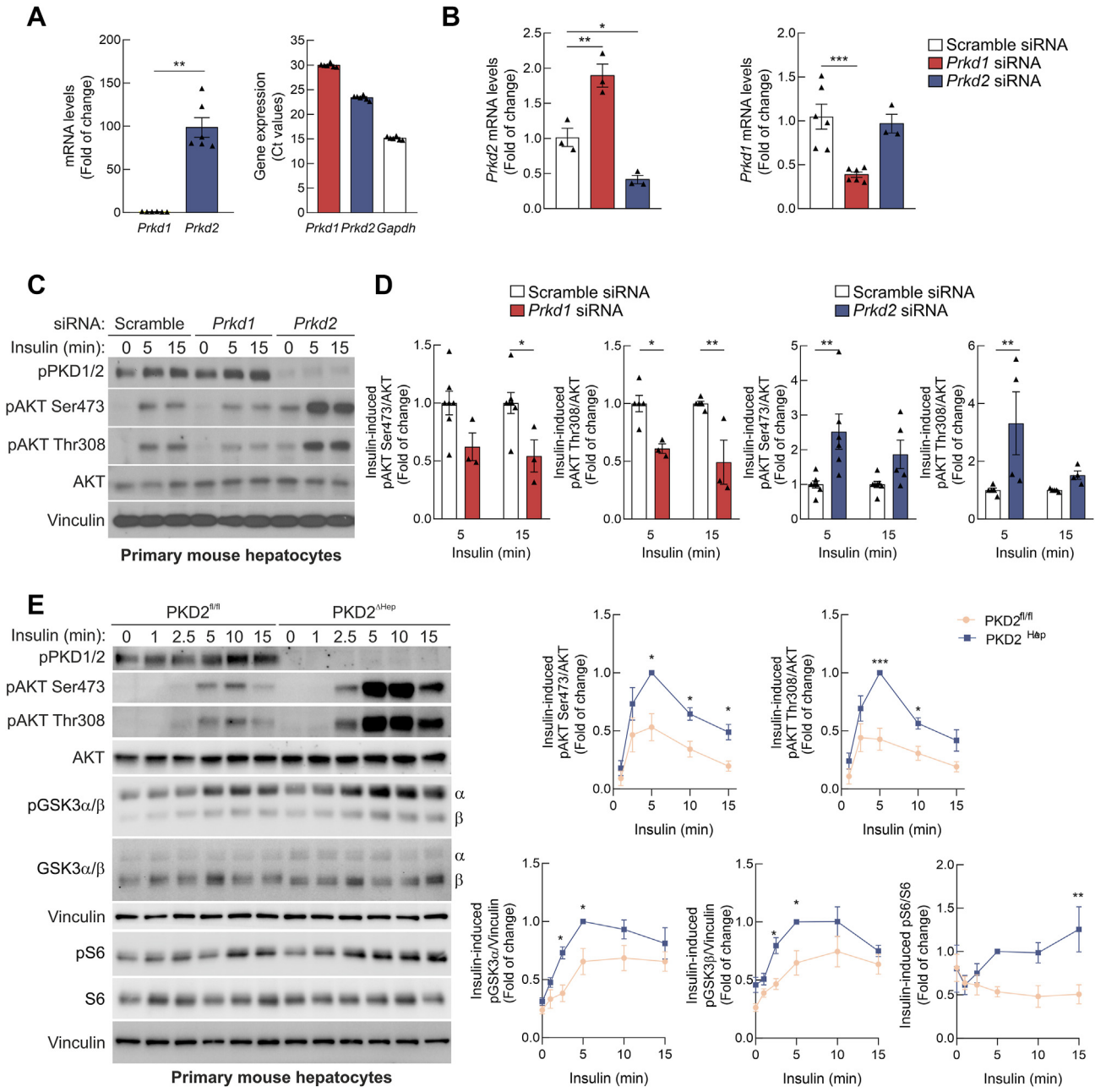

Figure 1: Genetic depletion of PKD modulates insulin sensitivity. ***A***. (Left) *Prkd1* (red) and *Prkd2* (blue) mRNA levels in primary mouse hepatocytes normalized with *Gapdh* mRNA levels. (Right) *Prkd1*, *Prkd2* and *Gapdh* gene expression showed as Ct values. Values are mean ± SEM (n = 6). $^{**}p < 0.01$ vs *Prkd1* mRNA levels according to Student's t-test. ***B.*** *Prkd2* (left) and *Prkd1* (right) mRNA levels from primary mouse hepatocytes transfected with scramble, *Prkd1* or *Prkd2* siRNAs. *Actb* was used for normalization. Values are mean ± SEM (*Prkd2* mRNA, n = 3; *Prkd1* mRNA, n = 6 for scramble and *Prkd1* siRNAs, and n = 3 for *Prkd2* siRNA). $^{*}p < 0.05$, $^{**}p < 0.01$, $^{***}p < 0.001$ *versus* scramble siRNA according to One-way ANOVA with Bonferroni *post hoc* test. ***C.*** Primary mouse hepatocytes transfected with scramble, *Prkd1* or *Prkd2* siRNAs were stimulated with insulin (10 nM) at the indicated time points. pPKD1/2 and pAKT (Ser473 and Thr308) protein levels were analyzed by immunoblot. Total AKT and Vinculin were used as loading controls. ***D.*** Densitometric quantification of pAKT protein levels after insulin treatment in primary hepatocytes silenced with *Prkd1* (left) or *Prkd2* (right) siRNAs as in c. Values are mean ± SEM (left, n = 6 for scramble siRNA and n = 3 for *Prkd1* siRNA. Right, pAKT Ser473, n = 7 for scramble siRNA and n = 6 (5 min) and 5 (15 min) for *Prkd2* siRNA; pAKT Thr308, n = 5 for scramble siRNA and n = 4 for *Prkd2* siRNA). $^{*}p < 0.05$, $^{**}p < 0.01$ *versus* scramble siRNA according to Two-way ANOVA with Bonferroni *post hoc* test. ***E.*** $PKD2^{fl/fl}$ and $PKD2^{\Delta Hep}$ primary hepatocytes were stimulated with insulin (10 nM) at the indicated times. pPKD1/2, pAKT, pGSK3α/β and pS6 protein levels were analyzed by immunoblot. Total AKT, GSK3α/β, S6 and Vinculin were used as loading controls. Densitometric quantification of pAKT, pGSK3α/β and pS6 protein levels after insulin treatment. Values are mean ± SEM (n = 10 for pAKTs and n = 7 for pGSK3α/β, n = 4 for pS6). $^{*}p < 0.05$, $^{**}p < 0.01$, $^{***}p < 0.001$ *versus* $PKD2^{fl/fl}$ primary hepatocytes according to Two-way ANOVA with Bonferroni *post hoc* test.

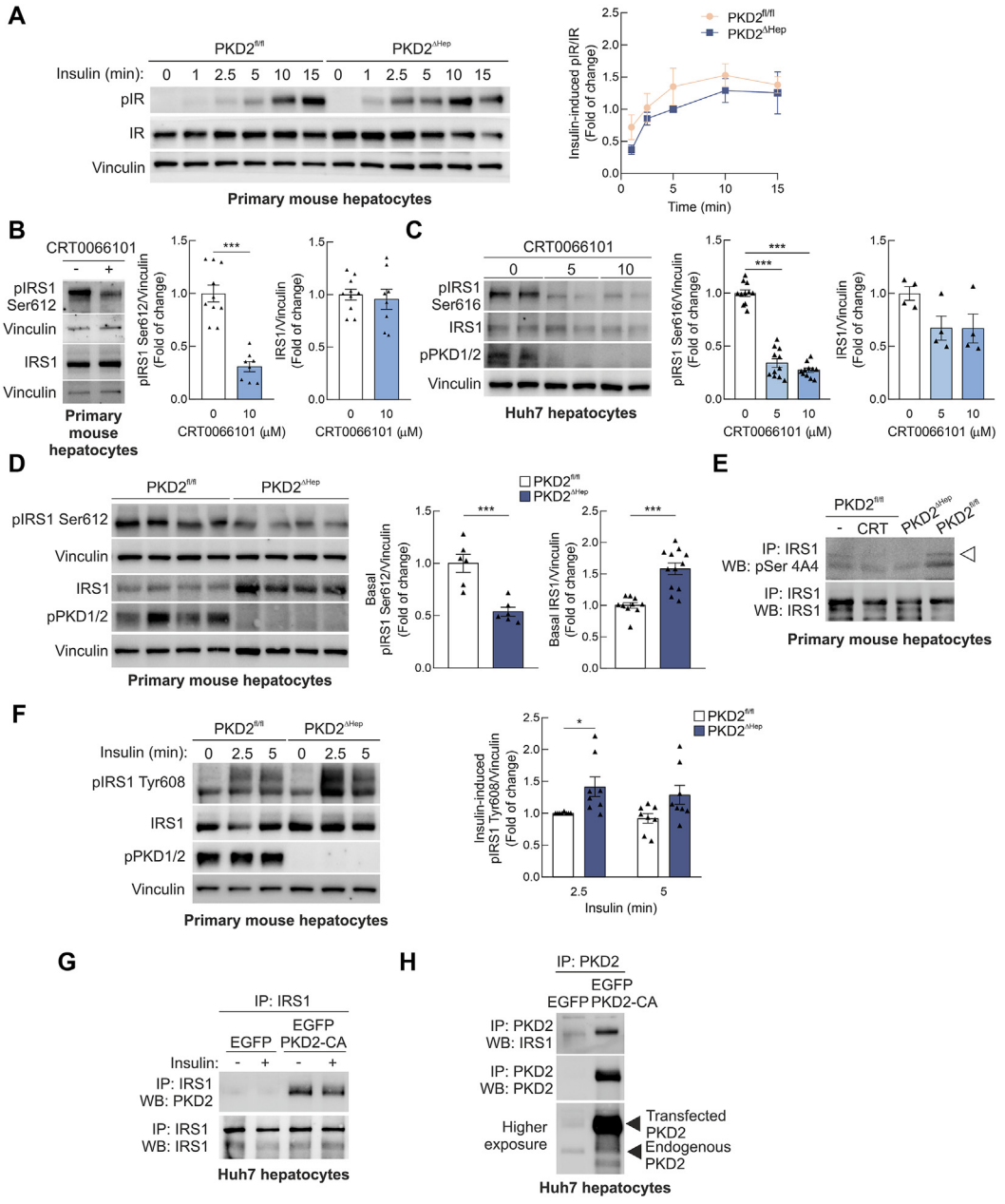

Figure 2: PKD2 participates in the control of IRS1 phosphorylation to modulate insulin sensitivity. ***A.*** PKD2$^{fl/fl}$ and PKD2$^{\Delta Hep}$ primary hepatocytes were stimulated with insulin (10 nM) at the indicated times. pIR and IR protein levels were analyzed by immunoblot. Total IR and Vinculin were used as loading controls. Densitometric quantification of pIR protein levels after insulin treatment. Values are mean ± SEM (n = 9). ***B.*** Western blot images showing pIRS1 Ser612 and total IRS1 protein levels from primary mouse hepatocytes treated with CRT0066101 (10 μM, 2 h). Vinculin was used as loading control. Densitometric quantification of pIRS1 Ser612 protein levels. Values are mean ± SEM (n = 10 for vehicle and n = 8 for CRT0066101). ***p < 0.001 *versus* vehicle according to Student's t-test. ***C.*** Western blot images showing pIRS1 Ser616, IRS1 and pPKD1/2 protein levels from Huh7 human hepatocytes treated with CRT0066101 (5 and 10 μM, 2 h). Vinculin was used as loading control. Densitometric quantification of pIRS1 Ser616 protein levels. Values are mean ± SEM (pSer616 IRS1, n = 11; IRS1, n = 4). ***p < 0.001 *versus* untreated according to One-way ANOVA with Bonferroni *post hoc* test. ***D.*** Western blot images showing pIRS1 Ser612, total IRS1 and pPKD1/2 protein levels from PKD2$^{fl/fl}$ and PKD2$^{\Delta Hep}$ primary hepatocytes. Vinculin was used as loading control. Densitometric quantification of pIRS1 Ser612 and total IRS1 protein levels. Values are mean ± SEM (pIRS1 Ser612, n = 6; IRS1, n = 10 for PKD2$^{fl/fl}$ and n = 12 for PKD2$^{\Delta Hep}$ hepatocytes). ***p < 0.001 *versus* PKD2$^{fl/fl}$ primary hepatocytes according to Student's t-test (pIRS1) and unpaired t test with Welch's correction (IRS1). ***E.*** IRS1 was immunoprecipitated from PKD2$^{fl/fl}$ primary hepatocytes treated or not with CRT0066101 (10 μM, 2 h) and from PKD2$^{\Delta Hep}$ primary hepatocytes. Total pSer residues and IRS1 levels were determined by Western blot. The arrow points pSer residues that disappear in the absence of PKD2. A representative experiment out of 3 is shown. ***F.*** PKD2$^{fl/fl}$ and PKD2$^{\Delta Hep}$ primary hepatocytes were stimulated with insulin (10 nM) at the indicated times. pIRS1 Tyr608 and total IRS1 protein levels were analyzed by immunoblot. Vinculin was used as loading controls. Densitometric quantification of pIRS1 Tyr608 protein levels after insulin treatment. Values are mean ± SEM (n = 8). *p < 0.05 *versus* PKD2$^{fl/fl}$ primary hepatocytes according to Two-way ANOVA with Bonferroni *post hoc* test. ***G.*** Huh7 human hepatocytes were transfected either EGFP or EGFP-PKD2-CA, a constitutively active form of human PKD2 fused to EGFP protein where Ser706 and Ser710 were mutated to glutamic acid to mimic serine phosphorylation. After 24 h, cells were serum-starved and stimulated with insulin (10 nM, 5 min). IRS1 was immunoprecipitated and PKD2 in the immunocomplexes was determined by Western blot. ***H.*** Huh7 human hepatocytes were transfected either EGFP or EGFP-PKD2-CA. After 24 h, both endogenous and transfected PKD2 were immunoprecipitated with the h-PKD2 antibody and IRS1 in the immunocomplexes was determined by Western blot.

hepatocytes using siRNA, interfering in parallel *Prkd1* (Figure 1B). Unexpectedly, despite of the low *Prkd1* expression in hepatocytes, its depletion by siRNA prominently raised *Prkd2* mRNA levels (Figure 1B, left) whereas *Prkd1* gene expression did not change upon *Prkd2* interference (Figure 1B, right). Notably, *Prkd2* silencing increased insulin-induced AKT phosphorylation while *Prkd1* siRNA decreased it (Figure 1C—D). As found in *Prkd1* siRNA experiments, primary hepatocytes from mice with hepatocyte-specific deletion of *Prkd1* (PKD1$^{\Delta Hep}$) showed a reduction in phospho-AKT levels (Supplementary Fig. 3a) and genetic deletion of *Prkd1* markedly increased PKD2 phosphorylation (Supplementary Fig. 3b,c). Of note, even though the antibody used can recognize phospho-PKD1/2, the band observed in hepatocytes by Western blot corresponds to PKD2 due to both the low *Prkd1* gene expression in these cells and the disappearance of the signal after *Prkd2* silencing (Figure 1C). In line with data using siRNAs, immortalized mouse hepatocytes efficiently transduced with *Prkd2* or scrambled shRNA lentivirus showed that *Prkd2* silencing increased AKT phosphorylation upon insulin stimulation (10 nM, 5 min) (Supplementary Fig. 4a,b).

To further confirm the relevance of PKD2 in hepatocyte insulin signaling we generated mice with specific deletion of PKD2 in hepatocytes (PKD2$^{\Delta Hep}$). Of note, PKD2 deficiency totally abolished the phospho-PKD1/2 signal in total or membrane protein lysates from primary hepatocytes, confirming again the low expression of PKD1 in these cells (Supplementary Fig. 5a,b). As shown in Figure 1E, primary hepatocytes from PKD2$^{\Delta Hep}$ male mice showed significantly higher phosphorylation levels of AKT and its downstream targets Glycogen Synthase Kinase 3 α/β (GSK3α/β) and Ribosomal Protein S6 (S6) upon insulin stimulation compared to PKD2$^{fl/fl}$ hepatocytes. Overall, these findings suggest that, in addition to PKD3 [22], targeting PKD2 might be therapeutically relevant in the context of insulin action in the liver.

3.2. PKD2 controls hepatocyte insulin signaling by modulating IRS1 phosphorylation

Since the analysis of IR tyrosine phosphorylation did not show differences in the response to insulin between PKD2$^{fl/fl}$ and PKD2$^{\Delta Hep}$ primary hepatocytes (Figure 2A), we explored the potential modulation of insulin signaling by PKD2 downstream IR and upstream AKT, particularly, at the level of insulin receptor substrate 1 (IRS1). Many studies have reported that IRS1 phosphorylation in serine residues triggers its proteosomal degradation and switches off insulin signaling causing insulin resistance [46,47]. As an initial approach we tested the impact of PKDs on IRS1 serine phosphorylation in primary mouse (Figure 2B) and human Huh7 (Figure 2C) hepatocytes exposed to CRT0066101, finding a significant reduction of IRS1 serine 612/616 (Ser612/616, rodent/human, respectively) phosphorylation. In this regard, a similar decrease in basal IRS1 Ser612 phosphorylation was observed in PKD2$^{\Delta Hep}$ primary hepatocytes concurrently with an elevation of total IRS1 protein levels (Figure 2D). IRS1 serine phosphorylation was also tested in primary hepatocytes by immunoprecipitation using a pan phospho-serine antibody. As shown in Figure 2E, while IRS1 was phosphorylated on serine residues in PKD2$^{fl/fl}$ hepatocytes, this phosphorylation was decreased in both CRT0066101-treated PKD2$^{fl/fl}$ primary hepatocytes and PKD2$^{\Delta Hep}$ primary hepatocytes. Since IRS1 has been shown to be phosphorylated by several protein kinases including IKKα/β, JNK1/2 and ERK1/2 [48—51], we analyzed whether these kinases might compensate for the loss of PKD2 in hepatocytes. As shown in Supplementary Fig. 5c, similar basal IKKα/β, JNK1/2 and ERK1/2 phosphorylation levels were found in PKD2$^{fl/fl}$ and PKD2$^{\Delta Hep}$ primary hepatocytes. Given the impact of PKD2 on IRS1 serine phosphorylation, we next tested if PKD2 deficiency affects insulin-induced IRS1 tyrosine phosphorylation, an issue not previously addressed with PKDs in hepatocytes. Results revealed that the absence of PKD2 enhanced insulin-induced IRS1 tyrosine 608 (Tyr608) phosphorylation (Figure 2F).

As our data point that PKD2 is involved in the regulation of the phosphorylation status of IRS1, we addressed a possible interaction between these two proteins. To this aim, IRS1-PKD2 association was analyzed in Huh7 hepatocytes overexpressing either EGFP or EGFP-PKD2-CA. Figure 2G shows PKD2-IRS1 co-immunoprecipitation regardless of insulin stimulation. Additionally, immunoprecipitation of either endogenous or transfected PKD2 in Huh7 cells confirmed this association (Figure 2H). Collectively, these results demonstrate that PKD2 modulates insulin signaling at the level of IRS1 in hepatocytes.

3.3. PKD2 overexpression in hepatocytes promotes insulin resistance

Next, we examined the effect of overexpressing PKD2 on insulin signaling in Huh7 hepatocytes and found a decrease in insulin-induced AKT phosphorylation (Figure 3A). Further, in order to evaluate whether PKD2 activation modulates insulin signaling *in vivo*, C57BL/6J male mice were injected AAV expressing constitutively active PKD2 (AAV-EGFP-PKD2-CA) or control AAV (AAV-Control). As shown in Figure 3B, human EGFP-PKD2-CA expression, assessed by Western blot, was detected in liver, but not in skeletal muscle. Mice overexpressing PKD2 in hepatocytes displayed similar body weight (BW) and plasma insulin levels as their age-matched AAV-control mice (Figure 3C and D). Neither glucose nor insulin tolerance tests (GTT and ITT, respectively) revealed differences among groups (Figure 3E and F). Next, pyruvate tolerance test (PTT) was performed to analyze the specific response of the liver, where PKD2 is overexpressed in hepatocytes, observing a significant pyruvate intolerance in AAV-EGFP-PKD2-CA-injected mice (Figure 3G).

We next explored how PKD2 activation impacts on insulin signaling in the liver. Strikingly, basal phosphorylation of IRS1 at Ser612 was enhanced when PKD2 was overexpressed in hepatocytes (Figure 3H) and, importantly, in response to insulin stimulation, IRS1 Tyr608 phosphorylation was decreased (Figure 3I). Moreover, insulin-induced AKT phosphorylation was reduced in AAV-EGFP-PKD2-CA livers compared to AAV-Control mice (Figure 3J), in agreement with the *in vitro* results. By contrast, in line with the ITT, insulin-induced AKT phosphorylation in skeletal muscle was comparable among groups (Figure 3K). Taken together, these results show that PKD2 activation in hepatocytes promotes molecular and metabolic signatures of insulin resistance in the liver.

3.4. PKD2$^{\Delta Hep}$ primary hepatocytes are more sensitive to insulin compared to PKD2$^{fl/fl}$ hepatocytes in an obesogenic environment

DG levels are increased in obesity and insulin resistance [52] and PKDs are activated by DG-signaling through PKCs activation. Thus, we examined PKD2 activation state in a lipid overload environment in hepatocytes treated with palmitic acid (PA) or in hepatocytes from mice fed a HFD, mimicking insulin resistance inherent to obesity and MASLD. As shown in Figure 4A, treatment with 600 μM PA for 1—4 h increased PKD2 phosphorylation. In a more physiopathological context, primary hepatocytes from HFD-fed mice showed an increase in PKD2 phosphorylation in parallel with an elevation in IRS1 Ser612 phosphorylation compared to hepatocytes from mice fed a CHD, without changes in total IRS1 protein levels (Figure 4B). A step further, *Prkd2* and *Prkd3* expression levels were determined in primary hepatocytes from CHD and HFD-fed mice from both genotypes (Figure 4C). As

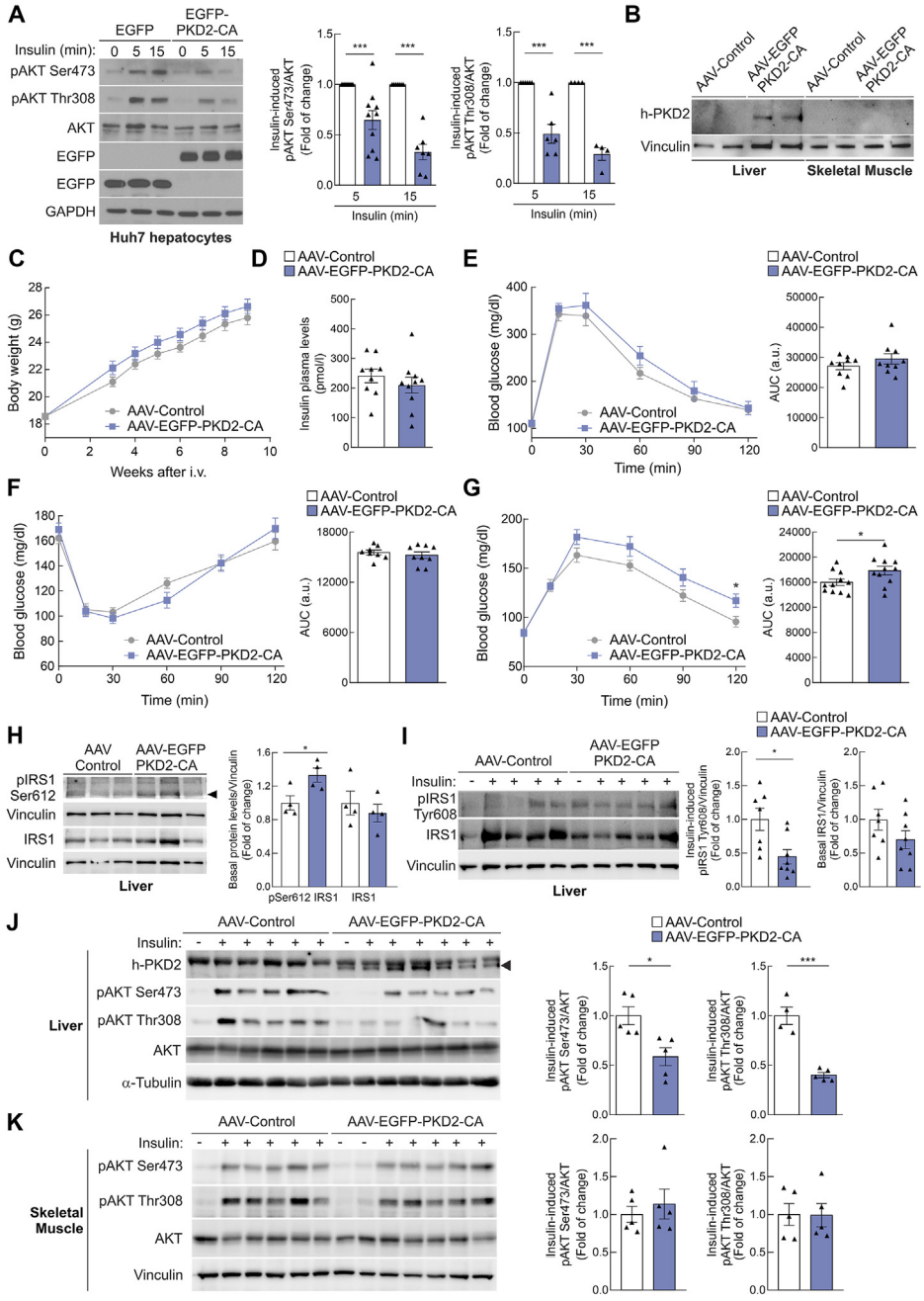

Figure 3: Overexpression of a constitutively active PKD2 mutant in hepatocytes promotes insulin resistance *in vitro* and *in vivo*. ***A***. Huh7 cells were transfected either EGFP or EGFP-PKD2-CA. After 24 h, cells were serum-starved and stimulated with insulin (10 nM, 5–15 min). pAKT (Ser473 and Thr308), total AKT and EGFP levels are shown. GAPDH was used as loading control. Values are mean ± SEM (pAKT Ser473, n = 10 for 5 min and n = 7 for 15 min; pAKT Thr308, n = 6 for 5 min and n = 4 for 15 min). ***p < 0.001 *versus* each EGFP condition according to Two-way ANOVA with Bonferroni *post hoc* test. ***B***. Four-week-old male mice were injected via tail vein AAV-EGFP-PKD2-CA or AAV-Control (0.5×10^{11} vp/ml). Western blot images from human PKD2 determination in liver and muscle extracts to corroborate human PKD2 overexpression in livers from AAV-EGFP-PKD2-CA mice. ***C.*** BW was monitored from week 3 to the end of the experiment at week 9 (n = 9 mice for AAV-Control and n = 10 mice for AAV-EGFP-PKD2-CA mice). ***D***. Plasma insulin levels were determined in AAV-EGFP-PKD2-CA or AAV-Control mice in the fed state. Values correspond to mean ± SEM (n = 9 mice for AAV-Control and n = 10 mice for AAV-EGFP-PKD2-CA mice). ***E–G.*** GTT (E), ITT (F) and PTT (G) were performed in 16-h (GTT, PTT) or 4-h (ITT) fasted mice injected (i.p.) D-glucose (2 g/kg), human insulin (0.75 U/kg) or sodium pyruvate (1.5 g/kg), respectively. Graphs depict the area under the curve (AUC) from GTT, ITT and PTT. Values correspond to mean ± SEM (GTT, n = 9 mice/group; ITT, n = 8 mice for AAV-Control and n = 9 mice for AAV-EGFP-PKD2-CA mice; PTT, n = 11 mice/group). *p < 0.05 *versus* AAV-Control mice according to Student's t-test. ***H.*** Phospho-IRS1 Ser612 (black arrow) and total IRS1 protein levels determined in 4 h-fasted AAV-EGFP-PKD2-CA or AAV-Control mice. Values correspond to mean ± SEM (n = 4 mice/group). *p < 0.05 *versus* AAV-Control mice according to Student's t-test. ***I,*** Four h-fasted AAV-EGFP-PKD2-CA or AAV-Control mice were i.p. injected 0.75 U/kg human insulin for 15 min and pIRS1 Tyr608 protein levels in liver were analyzed by immunoblot. Values are mean ± SEM (n = 7 mice for AAV-Control and n = 8 mice for AAV-EGFP-PKD2-CA mice). *p < 0.05 *versus* AAV-Control according to Student's t-test. ***J-K.*** pAKT (Ser473 and Thr308) protein levels were analyzed by immunoblot in liver (J) and muscle (K) extracts from mice treated as in I. Total AKT, α-Tubulin (J) and Vinculin (K) were used as loading controls. Densitometric quantification of pAKT (Ser473 and Thr308) protein levels after insulin treatment. Values are mean ± SEM (liver, n = 5 mice/group for pAKT Ser473 and n = 4 mice for AAV-Control and n = 5 mice for AAV-EGFP-PKD2-CA mice for pAKT Thr308; muscle, n = 5 mice/group). *p < 0.05, ***p < 0.001 *versus* AAV-Control according to Student's t-test.

expected, a marked reduction in *Prkd2* mRNA levels was found in PKD2$^{\Delta Hep}$ primary hepatocytes in both dietary conditions. Importantly, primary hepatocytes from HFD-fed PKD2$^{fl/fl}$ mice showed a significant *Prkd2* mRNA up-regulation compared to those from CHD-fed PKD2$^{fl/fl}$ mice whereas no changes in *Prkd3* mRNA levels were observed. Next, we examined the impact of hepatocyte PKD2 deficiency on insulin signaling under this pathological condition. Concerning IRS1, as previously shown in hepatocytes from CHD-fed mice (Figure 2D), hepatocytes from HFD-fed PKD2$^{\Delta Hep}$ mice presented reduced IRS1 Ser612 phosphorylation and higher total IRS1 protein levels under basal conditions (Figure 4D). Moreover, insulin-induced IRS1 Tyr608 and AKT phosphorylation was enhanced in hepatocytes from HFD-fed PKD2$^{\Delta Hep}$ mice compared to PKD2$^{fl/fl}$ mice (Figure 4E). In contrast, analysis of primary hepatocytes from HFD-fed PKD1$^{\Delta Hep}$ mice revealed that PKD1 deficiency worsened insulin signaling, suggesting that PKD2 upregulation in hepatocytes lacking PKD1 might account for this effect (Supplementary Fig. 6). Altogether, these results show that the loss of PKD2 in hepatocytes significantly improves insulin signaling upon lipid overload.

3.5. Hepatocyte-specific PKD2 deficiency ameliorates HFD-induced insulin resistance in male mice

Given that lipid overload and insulin resistance are the "first hit" for MASLD progression, we examined metabolic parameters in PKD2$^{fl/fl}$ and PKD2$^{\Delta Hep}$ male mice fed a HFD for 14 weeks. As expected, PKD2$^{\Delta Hep}$ mice showed specific deletion of PKD2 in the liver, but not in the brain as a control tissue where this isoform is highly expressed (Figure 5A). Notably, the results revealed elevated *Prkd2* mRNA levels in the liver from PKD2$^{fl/fl}$ mice fed a HFD compared to their lean counterparts fed a CHD (Figure 5B), in agreement with the results in primary hepatocytes (Figure 4C). Concerning the other PKD family members, reduced hepatic *Prkd3* expression was found in PKD2$^{fl/fl}$ obese mice, whereas *Prkd1* remained unchanged (Figure 5B). Since no differences in *Prkd3* expression levels were found in primary hepatocytes from PKD2$^{fl/fl}$ lean or obese mice (Figure 4C), the decrease in liver tissue is likely attributable to non-parenchymal liver cells. In addition, similarly to what was found in primary hepatocytes (Figure 4B), PKD2 phosphorylation was increased in livers from HFD-fed PKD2$^{fl/fl}$ mice (Figure 5C). Next, *Prkd2* and *Prkd3* mRNA levels were determined in livers from PKD2$^{\Delta Hep}$ HFD-fed mice and Figure 5D shows reduced *Prkd2* expression levels in livers from PKD2$^{\Delta Hep}$ mice compared to those of PKD2$^{fl/fl}$ mice as expected, and also a slight decrease in *Prkd3*. As similar *Prkd3* mRNA levels were found in primary hepatocytes from HFD-fed PKD2$^{fl/fl}$ and PKD2$^{\Delta Hep}$ mice (Figure 4C), its decrease in the liver of PKD2$^{\Delta Hep}$ mice might be also related to the contribution of non-parenchymal liver cells. Overall, our data suggest higher PKD2 activity in the liver from obese mice.

The evaluation of BW in male mice from both genotypes under HFD revealed similar weight gain compared to their respective CHD-fed mice (Figure 5E). Next, food intake, blood glucose and plasma insulin levels were determined in CHD and HFD-fed PKD2$^{fl/fl}$ and PKD2$^{\Delta Hep}$ mice (Figure 5F–H). As expected, significant differences were observed due to the HFD administration; however, these parameters were comparable among genotypes. Likewise, no differences in the HOMA-IR were found between PKD2$^{fl/fl}$ and PKD2$^{\Delta Hep}$ male mice in either CHD or HFD condition (CHD-PKD2$^{fl/fl}$: 1.42 $\pm$ 0.07; CHD-PKD2$^{\Delta Hep}$: 1.67 $\pm$ 0.08; HFD-PKD2$^{fl/fl}$: 10.96 $\pm$ 1.13; HFD-PKD2$^{\Delta Hep}$: 10.74 $\pm$ 1.23 (n = 6–14)). Moreover, BW gain, food intake, blood glucose, and plasma insulin levels were similar in PKD2$^{fl/fl}$ and PKD2$^{\Delta Hep}$ female mice fed a HFD (Supplementary Fig. 7a–d). Consistently, respiratory exchange ratio (RER), energy expenditure (EE) or total spontaneous locomotor activity were not affected by hepatocyte-specific deletion of PKD2 in male or female mice on a HFD (Supplementary Fig. 8).

Next, metabolic tests were conducted in CHD and HFD-fed PKD2$^{fl/fl}$ and PKD2$^{\Delta Hep}$ mice. Initially, we compared the effect of diet (CHD or HFD) in glucose, insulin and pyruvate tolerance in each genotype. As depicted in Fig. 5I, the impairment in glucose tolerance induced by the obesogenic diet was comparable in the two genotypes as reflected in their respective AUC of the GTT. Moreover, both ITT and PTT revealed less insulin and pyruvate intolerance in HFD-fed PKD2$^{\Delta Hep}$ mice (Figure 5J and K). We also compared the effect of the genotype (PKD2$^{fl/fl}$ and PKD2$^{\Delta Hep}$) in mice fed either CHD or HFD (Supplementary Fig. 9a–c). Whereas no differences in the GTT, ITT or PTT were found in mice fed a CHD, a slight improvement in glucose tolerance in the first 15 min was found in PKD2$^{\Delta Hep}$ mice fed a HFD, as well as enhanced glucose cleareance in the ITT and better pyruvate tolerance. No differences among genotypes were found in mRNA levels of the gluconeogenic enzymes *G6pc* and *Pck1* in either CHD or HFD (Supplementary Fig. 9d).

Thereafter, we addressed the impact of PKD2 deficiency in hepatocytes on insulin signaling in the liver tissue. First, IRS1 serine phosphorylation levels were analyzed in livers of HFD-fed PKD2$^{fl/fl}$ and PKD2$^{\Delta Hep}$ mice. As shown in Figure 6A, a significant reduction in IRS1 Ser612 phosphorylation was found in livers lacking hepatocyte PKD2, in line with the results in primary hepatocytes (Figure 4C). Accordingly, insulin-induced IRS1 Tyr608 and AKT phosphorylation was enhanced in livers of HFD-fed PKD2$^{\Delta Hep}$ mice whereas IR phosphorylation remained unchanged (Figure 6B). Also, AKT downstream targets were examined and, as shown in Figure 6C, a marked increase in the phosphorylation levels of GSK3α/β, Forkhead Box O1 (FOXO1) and S6 was found in livers from PKD2$^{\Delta Hep}$ mice. Of note, beside the enhanced insulin signaling in PKD2$^{\Delta Hep}$ hepatocytes (Figure 1E), no differences in hepatic AKT phosphorylation were found in mice fed a CHD (Supplementary Fig. 10) although glycogen content was higher in livers from CHD-fed PKD2$^{\Delta Hep}$ mice (Figure 6D). By contrast no differences among genotypes were found in hepatic glycogen content in mice fed a HFD. Regarding skeletal muscle, insulin-induced IR and AKT phosphorylation was comparable among groups upon HFD administration (Figure 6E). The beneficial effects of hepatocyte-specific deletion of PKD2 in males on glucose homeostasis and *in vivo* insulin responsiveness were absent in female mice fed a HFD (Supplementary Fig. 7e–h). At the molecular level, HFD administration in female mice did not change hepatic *Prkd2* and *Prkd3* mRNA levels nor increased phospho-PKD2 levels when compared to their CHD-fed counterparts (Supplementary Fig. 7i). Overall, our data indicate that PKD2 regulates hepatic insulin signaling in male mice.

3.6. Deletion of PKD2 does not affect hepatic steatosis in male mice fed a HFD

To examine pathophysiological features in the tissue, we performed H&E and Oil Red O (ORO) staining in liver sections from HFD-fed PKD2$^{fl/fl}$ and PKD2$^{\Delta Hep}$ mice (Figure 7A). Analysis of the NAS score, which evaluates the grade of steatosis, lobular inflammation and hepatocyte ballooning, revealed no differences between genotypes upon HFD administration (Figure 7B). In this line, no significant changes were found in plasma TG and cholesterol levels, whereas a reduction in circulating free FAs was found (Figure 7C). Likewise, ALT activity remained unchanged (Figure 7D). Moreover, HFD-fed PKD2$^{\Delta Hep}$ and PKD2$^{fl/fl}$ females showed comparable plasma TG, cholesterol, free FAs

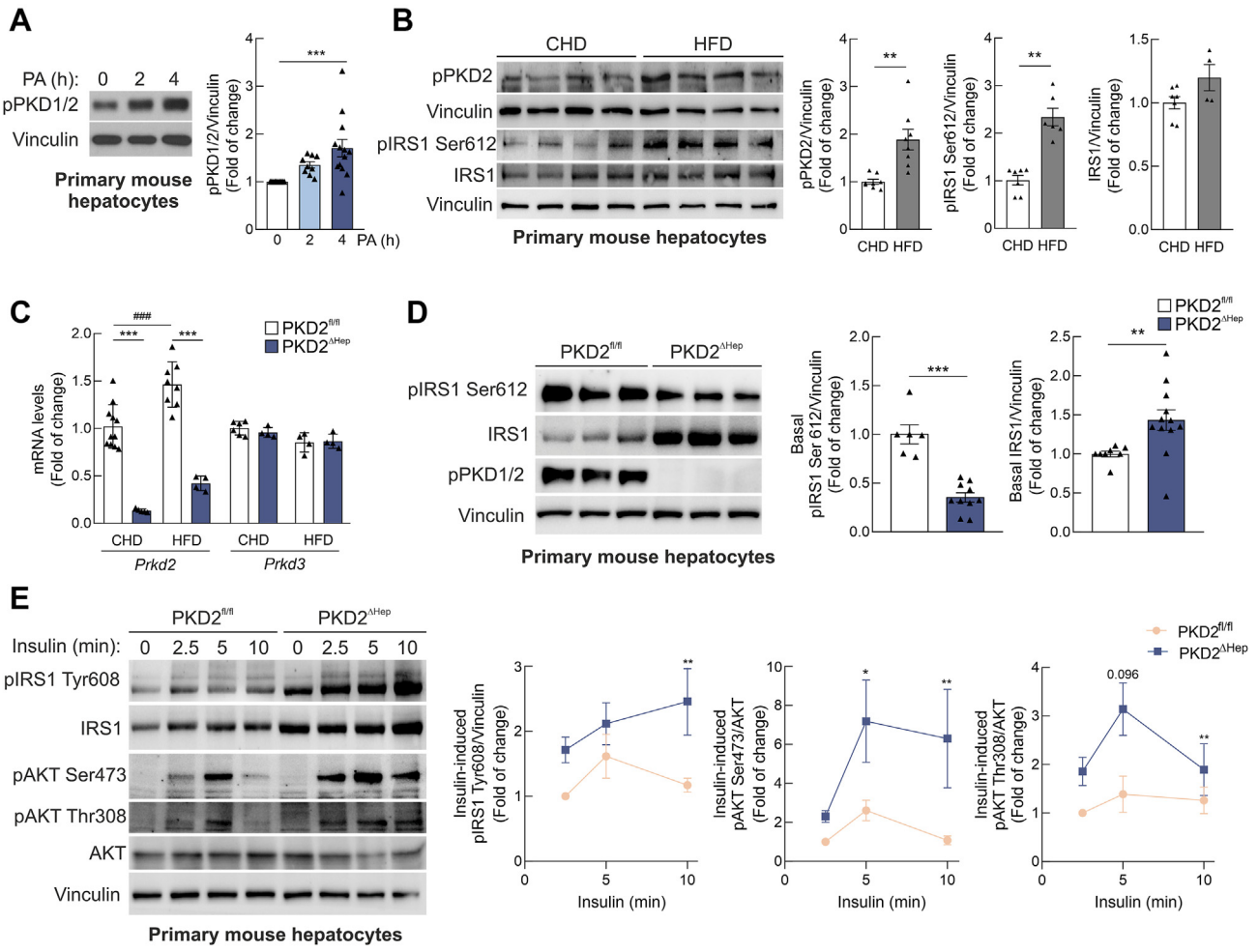

Figure 4: PKD2$^{\Delta Hep}$ *primary hepatocytes from HFD-fed mice exhibit improved insulin sensitivity compared to PKD2$^{fl/fl}$ hepatocytes.* *A*. Primary mouse hepatocytes from PKD2$^{fl/fl}$ mice were treated with 600 μM PA in 5.5 mM glucose DMEM supplemented with 2.5% FBS and 0.5% free-FA BSA for 2 and 4 h, and pPKD1/2 protein were determined. Vinculin was used as loading control. Densitometric quantification of pPKD1/2 protein levels. Values are mean ± SEM (n = 9–13). ***p < 0.001 *versus* time 0 according to One-way ANOVA with Bonferroni *post hoc* test. ***B.*** Protein levels of pPKD2, pIRS1 Ser612 and total IRS1 in primary hepatocytes isolated from CHD- and HFD-fed mice. Vinculin was used as loading control. Densitometric quantification of pPKD2, pIRS1 Ser612 and total IRS1 protein levels. Values are mean ± SEM (pPKD2 and pIRS1 Ser612, n = 7 for CHD hepatocytes and n = 6 for HFD hepatocytes; IRS1, n = 7 for CHD hepatocytes and n = 4 for HFD hepatocytes). **p < 0.01 *versus* CHD hepatocytes according to Student's t-test. ***C.*** *Prkd2* (left) and *Prkd3* (right) mRNA levels of primary mouse hepatocytes from PKD2$^{fl/fl}$ and PKD2$^{\Delta Hep}$ mice fed a CHD or HFD. *Rplp0* was used for normalization. Values are mean ± SEM (*Prkd2*: CHD-PKD2$^{fl/fl}$, n = 6, CHD-PKD2$^{\Delta Hep}$, n = 5, HFD-PKD2$^{fl/fl}$, n = 8, HFD-PKD2$^{\Delta Hep}$, n = 4; *Prkd3*: n = 6 for CHD-PKD2$^{fl/fl}$ and n = 4 for HFD-PKD2$^{fl/fl}$, CHD- and HFD-PKD2$^{\Delta Hep}$). ***p < 0.001 *versus* PKD2$^{fl/fl}$ hepatocytes and ###p < 0.001 *versus* CHD hepatocytes according to Two-way ANOVA with Bonferroni *post hoc* test. ***D.*** Basal protein levels of pIRS1 Ser612, IRS1 and pPKD1/2 in PKD2$^{fl/fl}$ and PKD2$^{\Delta Hep}$ primary hepatocytes isolated from HFD-fed mice. Vinculin was used as loading control. Densitometric quantification of pIRS1 Ser612 and IRS1 protein levels. Values are mean ± SEM (pIRS1 Ser612, n = 6 for PKD2$^{fl/fl}$ and n = 10 for PKD2$^{\Delta Hep}$; IRS1, n = 8 for PKD2$^{fl/fl}$ and n = 12 for PKD2$^{\Delta Hep}$). **p < 0.01, ***p < 0.001 *versus* PKD2$^{fl/fl}$ hepatocytes according to Student's t-test. ***E.*** PKD2$^{fl/fl}$ and PKD2$^{\Delta Hep}$ primary hepatocytes isolated from HFD-fed mice were stimulated with insulin (10 nM, 2.5–10 min). pIRS1 Tyr608, IRS1 and pAKT (Ser473 and Thr308) protein levels were analyzed by immunoblot. Total AKT and Vinculin were used as loading controls. Densitometric quantification of pIRS1 and pAKT protein levels after insulin treatment. Values are mean ± SEM (IRS1, n = 7 for PKD2$^{fl/fl}$ and n = 9 for PKD2$^{\Delta Hep}$; pIRS1 Tyr608, n = 7 for PKD2$^{fl/fl}$ and n = 11 for PKD2$^{\Delta Hep}$; pAKT Ser473, n = 9 for PKD2$^{fl/fl}$ and n = 13 for PKD2$^{\Delta Hep}$; pAKT Thr308, n = 8 for PKD2$^{fl/fl}$ and n = 12 for PKD2$^{\Delta Hep}$ primary hepatocytes). *p < 0.05, **p < 0.01 *versus* PKD2$^{fl/fl}$ primary hepatocytes according to Two-way ANOVA with Bonferroni *post hoc* test.

and ALT activity, as well as intrahepatic TG levels and NAS score (Supplementary Fig. 11).

Given the effect of insulin resistance on metabolic pathways that regulate lipid species content, lipidomic analysis was conducted to decipher possible differences in the remodeling of hepatic lipid species in HFD-fed PKD2$^{\Delta Hep}$ and PKD2$^{fl/fl}$ male mice. The Principal Component Analysis (PCA) confirmed the clustering of the samples in the experimental groups (Supplementary Fig. 12). A total of 84 lipid species presented significant variations in livers from HFD-fed PKD2$^{\Delta Hep}$ mice compared to PKD2$^{fl/fl}$ mice, among which most were decreased in HFD-fed PKD2$^{\Delta Hep}$ mice (Figure 8A and Table 2). In this regard, significant reductions were found in some FAs, phospholipids (PLs) and sphingomyelins, among others. However, 6 DG species (DG (16:0_18:3_0:0), DG (16:1_18:1_0:0), DG (16:1_18:2_0:0), DG (32:1), DG (34:1) and DG (34:2)) were elevated in livers from PKD2$^{\Delta Hep}$ mice. Notably, no significant changes were found in the 51 TG species analyzed (Figure 8A and Table 3). This metabolic rewiring in lipid metabolism was not observed when total concentrations of TGs, DGs or PLs were analyzed (Figure 8B), suggesting that the differences found in some lipid species in PKD2$^{\Delta Hep}$ livers do not affect lipid homeostasis.

One of the most important metabolic processes regulating hepatic lipid content is the mitochondrial fatty acid oxidation (FAO) which was

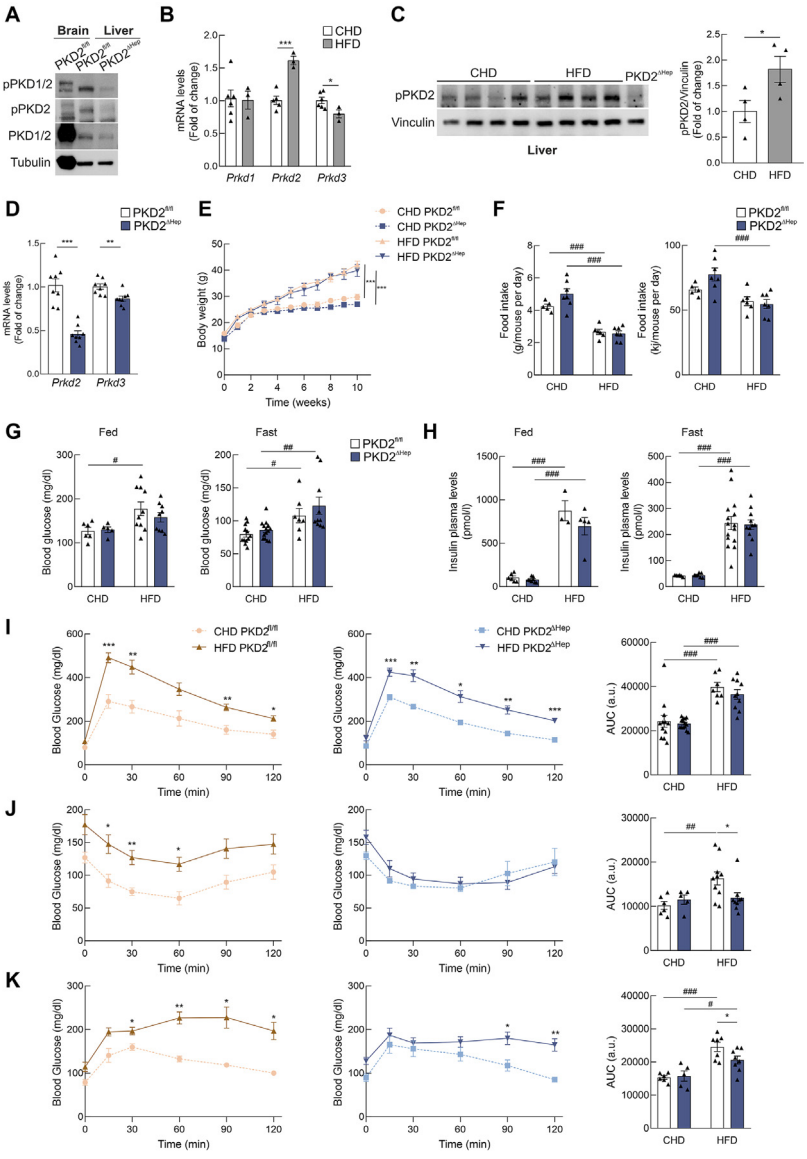

Figure 5: PKD2 deficiency in hepatocytes ameliorates HFD-induced insulin resistance in male mice. ***A***. Western blot images of pPKD1/2, pPKD2 and total PKD1/2 protein levels in brain and liver extracts to assess PKD2 depletion in livers from PKD2$^{\Delta Hep}$ mice. α-Tubulin was used as loading controls. ***B.*** *Prkd1*, *Prkd2* and *Prkd3* mRNA levels in livers from CHD- and HFD-fed (14 weeks) PKD2$^{fl/fl}$ male mice normalized with *Rplp0* mRNA levels. Values are mean ± SEM (*Prkd1*, n = 6 for CHD-fed mice and n = 3 for HFD-fed mice; *Prkd2*, n = 5 for CHD-fed mice and n = 3 for HFD-fed mice; *Prkd3*, n = 6 for CHD-fed mice and n = 3 for HFD-fed mice). *p < 0.05, ***p < 0.001 *versus* CHD-fed mice according to Student's t-test. ***C.*** Western blot images of pPKD2 protein levels in liver extracts from CHD- and HFD-fed (14 weeks) PKD2$^{fl/fl}$ male mice. Vinculin was used as a loading control. Densitometric quantification of pPKD2 protein levels. Values are mean ± SEM (n = 4 mice/group). *p < 0.05 *versus* CHD-fed mice according to Student's t-test. ***D.*** *Prkd2* (left) and *Prkd3* (right) mRNA levels of HFD-fed PKD2$^{fl/fl}$ and PKD2$^{\Delta Hep}$ mice. *Rplp0* was used for normalization. Values are mean ± SEM (n = 8). **p < 0.01, ***p < 0.001 *versus* PKD2$^{fl/fl}$ according to Student's t-test. ***E.*** Eight-week-old PKD2$^{fl/fl}$ and PKD2$^{\Delta Hep}$ male mice were fed a CHD or a HFD for 14 weeks. BW was monitored up to week 10 of HFD, time-point at which metabolic tests were performed. Values are mean ± SEM (CHD: n = 3 for PKD2$^{fl/fl}$ mice and n = 6 for PKD2$^{\Delta Hep}$ mice; HFD: n = 3 for PKD2$^{fl/fl}$ mice and n = 5 for PKD2$^{\Delta Hep}$ mice). , ***p < 0.001 *versus* CHD, according to Two-way ANOVA with Bonferroni *post hoc* test. ***F.*** Food intake of CHD- and HFD-fed PKD2$^{fl/fl}$ and PKD2$^{\Delta Hep}$ mice at the end of the experiment. Values are expressed as g/mouse/day and kj/mouse/day and are mean ± SEM (CHD: n = 5 for PKD2$^{fl/fl}$ mice and n = 7 for PKD2$^{\Delta Hep}$ mice; HFD: n = 6 for PKD2$^{fl/fl}$ mice and n = 7 for PKD2$^{\Delta Hep}$ mice). ***G.*** Blood glucose determined in either fed or 16 h-fasted CHD- and HFD-fed PKD2$^{fl/fl}$ and PKD2$^{\Delta Hep}$ mice. Values are mean ± SEM (CHD, fed, n = 6 for PKD2$^{fl/fl}$ mice and n = 5 for PKD2$^{\Delta Hep}$ mice; fast, n = 12 for PKD2$^{fl/fl}$ mice and n = 14 for PKD2$^{\Delta Hep}$ mice; HFD, fed, n = 10 for PKD2$^{fl/fl}$ mice and n = 9 for PKD2$^{\Delta Hep}$ mice; fast, n = 7 for PKD2$^{fl/fl}$ mice and n = 10 for PKD2$^{\Delta Hep}$ mice). ***H.*** Plasma insulin levels determined in fed and fasted PKD2$^{fl/fl}$ and PKD2$^{\Delta Hep}$ mice fed either CHD or HFD. Values are mean ± SEM (CHD, fed, n = 6 for PKD2$^{fl/fl}$ mice and n = 8 for PKD2$^{\Delta Hep}$ mice; fast, n = 7; HFD, fed, n = 3 for PKD2$^{fl/fl}$ mice and n = 5 for PKD2$^{\Delta Hep}$ mice; fast, n = 15 for PKD2$^{fl/fl}$ mice and n = 11 for PKD2$^{\Delta Hep}$ mice). For F-H, #p < 0.05, ##p < 0.01, ###p < 0.001 *versus* CHD according to Two-way ANOVA with Bonferroni *post hoc* test. ***I-K.*** GTT (I), ITT (J) and PTT (K) were performed in 16-h (GTT, PTT) or 4-h (ITT) fasted mice injected (i.p.) D-glucose (2 g/kg), human insulin (0.75 U/kg) or sodium pyruvate (1.5 g/kg), respectively. Bar graphs depict the area under the curve (AUC) from GTT, ITT and PTT. Values correspond to mean ± SEM (GTT: CHD, n = 12 for PKD2$^{fl/fl}$ mice and n = 14 for PKD2$^{\Delta Hep}$ mice; HFD, n = 7 for PKD2$^{fl/fl}$ mice and n = 10 for PKD2$^{\Delta Hep}$ mice; ITT: CHD, n = 6 for PKD2$^{fl/fl}$ mice and n = 5 for PKD2$^{\Delta Hep}$ mice; HFD, n = 10 for PKD2$^{fl/fl}$ mice and n = 9 for PKD2$^{\Delta Hep}$ mice; PTT: CHD, n = 6 for PKD2$^{fl/fl}$ mice and n = 5 for PKD2$^{\Delta Hep}$ mice; HFD, n = 7 for PKD2$^{fl/fl}$ mice and n = 8 for PKD2$^{\Delta Hep}$ mice). For time-course studies, statistical analysis was performed by Two-way repeated measurements ANOVA or by fitting a mixed model followed by a Bonferroni *post hoc* test. *p < 0.05, **p < 0.01, ***p < 0.001 *versus* CHD-fed mice. For AUC, *p < 0.05 *versus* HFD-fed PKD2$^{fl/fl}$ mice, #p < 0.05, ##p < 0.01, ###p < 0.001 *versus* CHD condition, according to Two-way ANOVA with Bonferroni *post hoc* test.

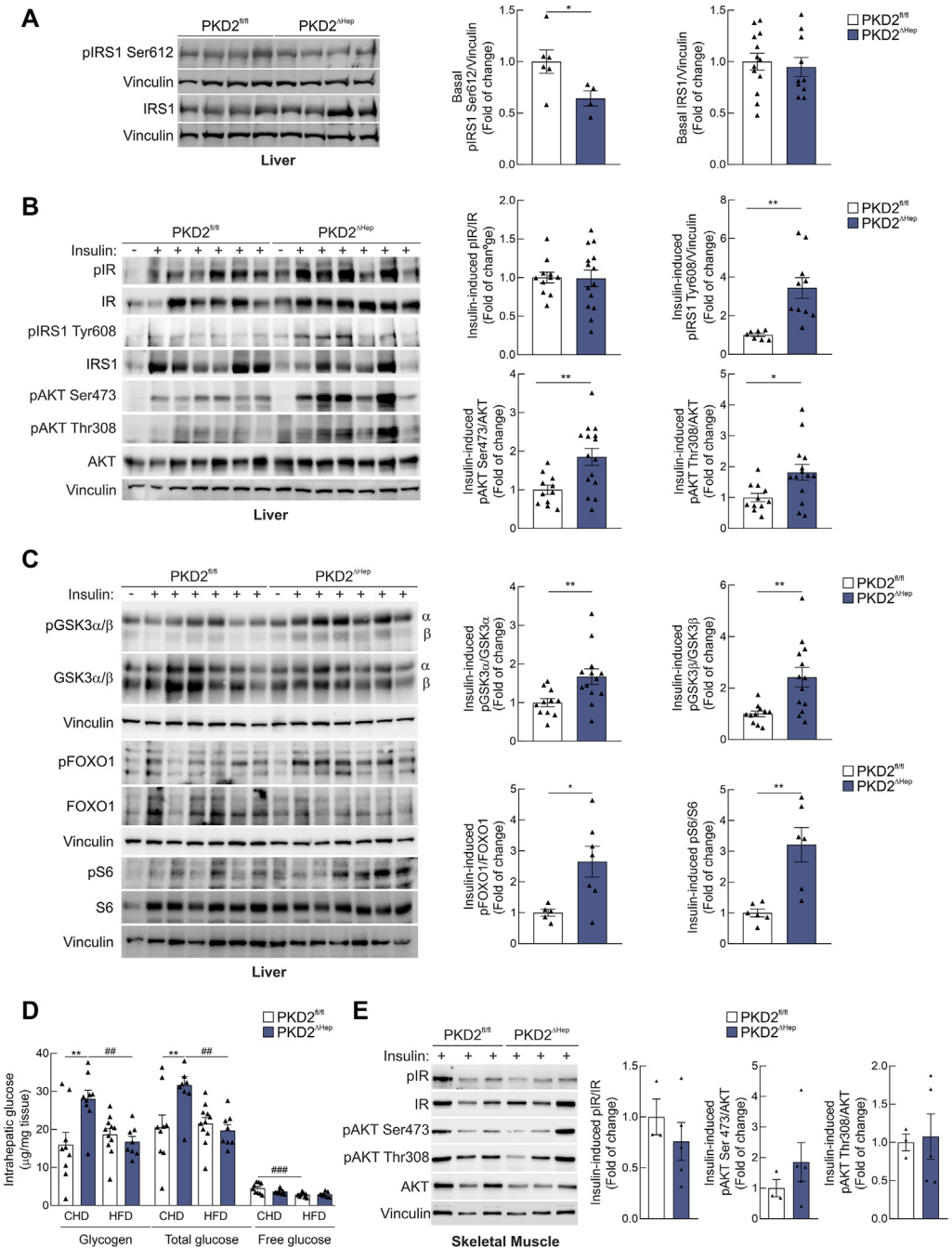

Figure 6: PKD2 deficiency in hepatocytes potentiates hepatic insulin responses after HFD administration in male mice. ***A***. Eight-week-old PKD2$^{fl/fl}$ and PKD2$^{\Delta Hep}$ male mice were fed a HFD for 14 weeks. Basal Ser612 IRS1 phosphorylation and total IRS1 levels were analyzed**.** Vinculin was used as loading control. Densitometric quantification of pIRS1 Ser612 and total IRS1 protein levels. Values are mean ± SEM (pIRS1, n = 6 for PKD2$^{fl/fl}$ mice and n = 4 for PKD2$^{\Delta Hep}$ mice; IRS1, n = 13 for PKD2$^{fl/fl}$ mice and n = 10 for PKD2$^{\Delta Hep}$ mice). *p < 0.05 *versus* PKD2$^{fl/fl}$ mice according to Student's t-test. ***B-C.*** Four h-fasted HFD-fed PKD2$^{fl/fl}$ or PKD2$^{\Delta Hep}$ mice were i.p. injected 0.75 U/kg human insulin for 15 min. In ***B***, pIR, pIRS1 Tyr608, pAKT (Ser473 and Thr308) protein levels were analysed by immunoblot in liver extracts. Total IR, AKT and Vinculin were used as loading controls. Densitometric quantification of pIR, pIRS1 Tyr608, pAKT (Ser473 and Thr308) protein levels after insulin treatment. Values are mean ± SEM (pIR, pAKT Ser473 and pAKT Thr308, n = 11 for PKD2$^{fl/fl}$ mice and n = 15 for PKD2$^{\Delta Hep}$ mice; pIRS1 Tyr608, n = 7 for PKD2$^{fl/fl}$ mice and n = 10 for PKD2$^{\Delta Hep}$ mice). *p < 0.05, **p < 0.01 *versus* PKD2$^{fl/fl}$ mice according to Student's t-test. In ***C***, pGSK3α/β, pFOX01 and pS6 protein levels were analyzed by immunoblot in liver extracts. Total GSK3α/β, FOX01, S6 and Vinculin were used as loading controls. Densitometric quantification of pGSK3α/β, pFOX01 and pS6 protein levels after insulin treatment. Values are mean ± SEM (pGSK3α/β: n = 11 for PKD2$^{fl/fl}$ mice and n = 13 for PKD2$^{\Delta Hep}$ mice; pFOX01, n = 5 for PKD2$^{fl/fl}$ mice and n = 7 for PKD2$^{\Delta Hep}$ mice; pS6, n = 6). *p < 0.05, **p < 0.01 *versus* PKD2$^{fl/fl}$ mice according to Student's t-test. ***D.*** Glycogen, total and free glucose levels in livers from CHD- and HFD (14 weeks)-fed PKD2$^{fl/fl}$ and PKD2$^{\Delta Hep}$ mice in the fed state. Values are mean ± SEM (for glycogen and total glucose, CHD n = 9, HFD n = 11 for PKD2$^{fl/fl}$ mice and n = 8 for PKD2$^{\Delta Hep}$ mice; for free glucose, CHD n = 9, HFD n = 11 for PKD2$^{fl/fl}$ mice and n = 9 for PKD2$^{\Delta Hep}$ mice). **p < 0.01 *versus* PKD2$^{fl/fl}$ mice, ##p < 0.01, ###p < 0.001 *versus* CHD condition, according to Two-way ANOVA with Bonferroni *post hoc* test. ***E.*** Protein levels of pIR and pAKT (Ser473 and Thr308) of muscle extracts from HFD-fed PKD2$^{fl/fl}$ or PKD2$^{\Delta Hep}$ mice treated as in b. Total IR, AKT and Vinculin were used as loading controls. Densitometric quantification of pIR and pAKT (Ser473 and Thr308) protein levels after insulin treatment. Values are mean ± SEM (n = 3 for PKD2$^{fl/fl}$ mice and n = 5 for PKD2$^{\Delta Hep}$ mice).

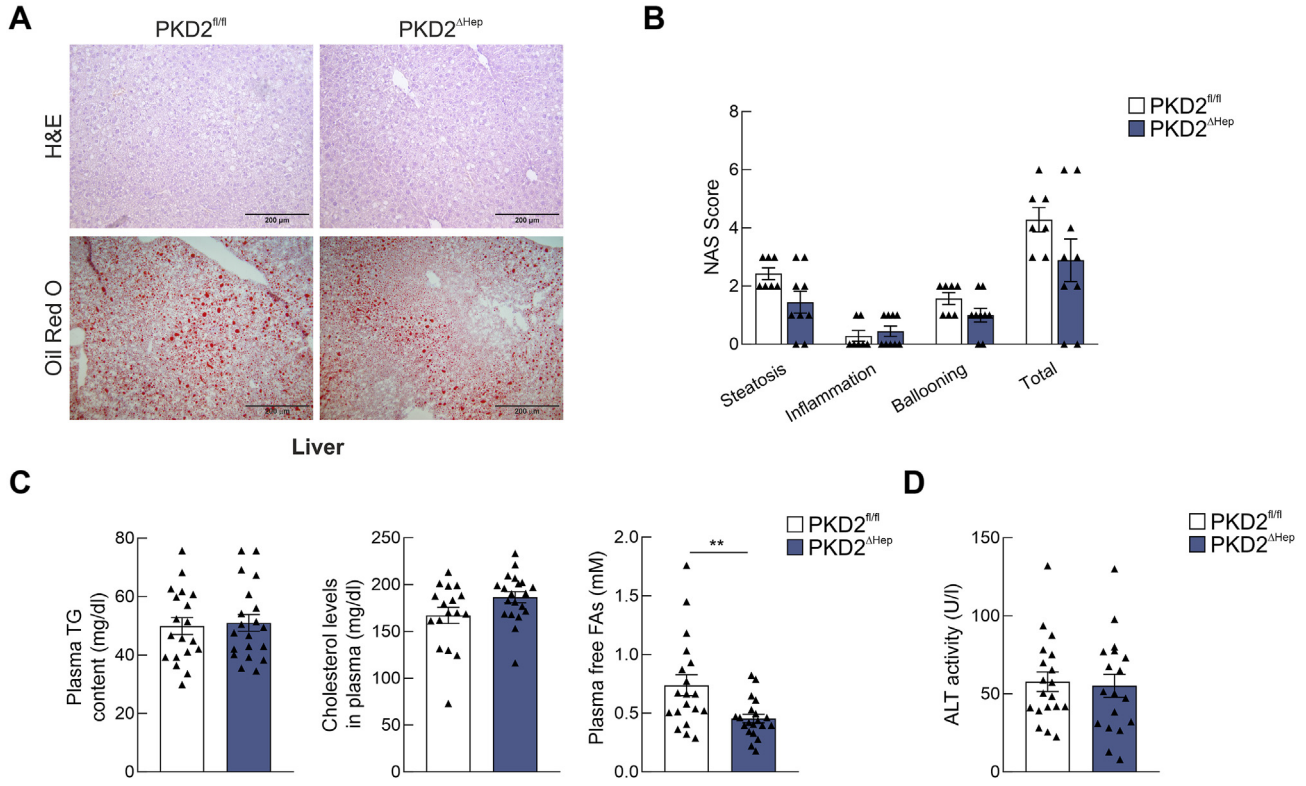

Figure 7: Deletion of PKD2 does not affect hepatic steatosis upon HFD administration. ***A***. H&E and Oil red O staining of liver sections from PKD2$^{fl/fl}$ and PKD2$^{\Delta Hep}$ mice fed a HFD for 14 weeks (20X, Scale bars = 200 μm). ***B.*** NAS Score. Values are mean ± SEM (n = 7 for PKD2$^{fl/fl}$ mice and n = 9 for PKD2$^{\Delta Hep}$ mice). ***C.*** Plasma TG levels (n = 19 for PKD2$^{fl/fl}$ mice and n = 20 for PKD2$^{\Delta Hep}$ mice), plasma cholesterol levels (n = 17 for PKD2$^{fl/fl}$ mice and n = 20 for PKD2$^{\Delta Hep}$ mice) and plasma free FAs (n = 19 for PKD2$^{fl/fl}$ mice and n = 20 for PKD2$^{\Delta Hep}$ mice) in PKD2$^{fl/fl}$ and PKD2$^{\Delta Hep}$ mice fed a HFD for 14 weeks. Values are mean ± SEM. $^{**}p < 0.01$ *versus* PKD2$^{fl/fl}$ mice according to Student's t-test. ***D.*** Plasma ALT activity (n = 19 for PKD2$^{fl/fl}$ mice and n = 18 for PKD2$^{\Delta Hep}$ mice) in PKD2$^{fl/fl}$ and PKD2$^{\Delta Hep}$ mice fed a HFD for 14 weeks. Values are mean ± SEM.

increased in the livers from HFD-fed PKD2$^{\Delta Hep}$ mice compared to PKD2$^{fl/fl}$ mice (Figure 8C). Moreover, *de novo* lipogenesis was comparable among genotypes as reflected by similar levels of FAs and FA incorporation into TGs (Figure 8D). These observations prompted us to examine AMP-activated protein kinase (AMPK) and acetyl-CoA carboxylase (ACC) activity since it is well known that AMPK inactivates ACC to promote FAO. After 14 weeks of HFD, no differences were found in pAMPK, pACC or fatty acid synthase (FAS) protein levels (Figure 8E). Overall, our data suggest that, although a remodeling in hepatic lipid fluxes is likely occurring in HFD-fed PKD2$^{\Delta Hep}$ mice, steatosis is not affected by PKD2 deficiency, at least in an early stage of MASLD.

4. DISCUSSION

In the last decade, multiple studies have shed light on the relevance and tissue-specificity of PKDs in metabolic homeostasis [53]. As reported, deletion of PKD1, the first identified [6,9] and the most studied isoform, in beta cells or adipocytes worsens or improves insulin sensitivity, respectively [19,20]. Regarding PKD2, its specific role in the intestine by regulating gut microbiota and lipid uptake in enterocytes has been recently reported [24]. Also, in C2C12 muscle cells PKD2 limits the beneficial effects of quercetin in palmitic acid-mediated oxidative stress [54]. Herein, we have demonstrated a novel role of PKD2 in the liver since its modulation in hepatocytes affects insulin signaling and glucose homeostasis in male mice.

In particular, our results uncover PKD2 as a negative modulator of hepatic insulin signaling, being this isoform more active in obese and insulin resistant mice. Data collected in PKD2$^{\Delta Hep}$ mice differ from those found by Xiao et al. in global PKD2 null mice [23] that displayed insulin resistance reflected by a marked reduction of insulin-induced AKT phosphorylation in both liver and skeletal muscle upon CHD feeding. Moreover, global PKD2 deficiency caused hyperinsulinemia, revealing that the lack of PKD2 in beta cells is sufficient to enhance insulin secretion which, in turn, evokes systemic insulin resistance. These findings, together with our data, reinforce the specific function of PKD2 in glucose metabolism depending on the target tissue.

The initial analysis of insulin signaling clearly showed enhanced AKT phosphorylation in mouse primary hepatocytes lacking PKD2 and in human hepatic cell lines in which PKDs were inhibited pharmacologically. Of note, Xiao et al. did not observe changes in insulin sensitivity in *Prkd2*-silenced Hepa1-6 cells [23]; however, a number of factors might contribute to these differences. In fact, it is known that hepatocarcinoma cell lines show lower insulin sensitivity, very low glucose production rates, aberrant expression of gluconeogenic genes and reduced FAS expression compared to primary hepatocytes [55,56]. In addition, the discrepancies between our current findings and this previous study might rely on the experimental settings. First, in our study experiments were conducted in hepatocytes cultured in DMEM containing 5.5 mM instead of 25 mM glucose, mimicking the plasma glucose concentration in the portal vein (4.50 ± 1.01 mM [57]). Second, in primary hepatocytes, maximal AKT phosphorylation

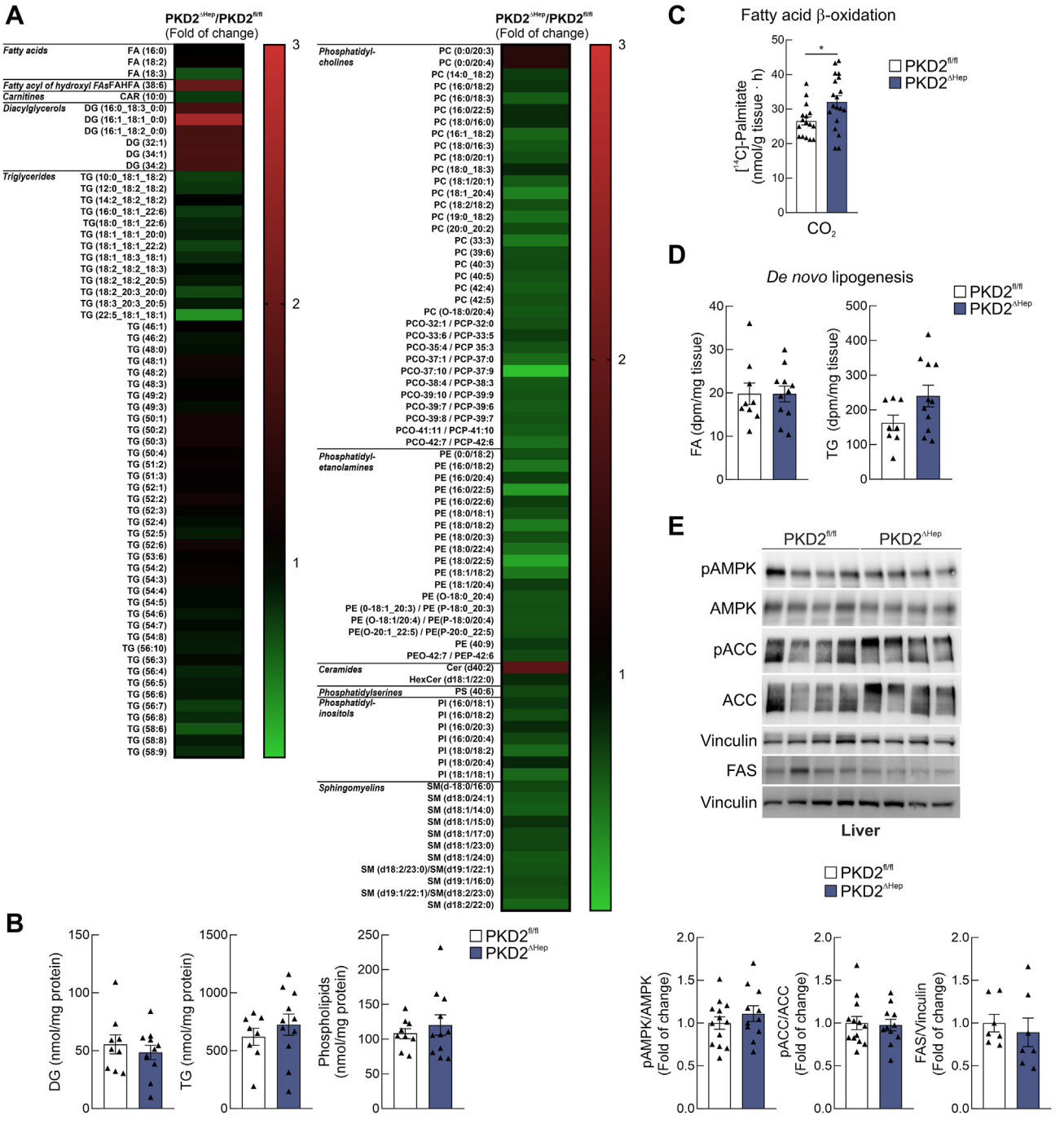

Figure 8: Hepatocyte PKD2 deficient male mice fed a HFD showed a remodeling of lipid species in the liver without changes in *de novo* lipogenesis. ***A***. Heatmap representing the fold of change of different lipid species in livers from HFD-fed (14 weeks) PKD2$^{\Delta Hep}$ mice *versus* livers from HFD-fed (14 weeks) PKD2$^{fl/fl}$ mice (n = 4 mice/group). The list of all the meaningful lipids based on the UVDA and MVDA results in both ionization modes are in Tables 2 and 3. ***B.*** DG, TG and PL hepatic content in livers from HFD-fed PKD2$^{fl/fl}$ and PKD2$^{\Delta Hep}$ mice (n = 9 for PKD2$^{fl/fl}$ mice and n = 11 for PKD2$^{\Delta Hep}$ mice). Values are mean ± SEM. ***C.*** Fatty acid β-oxidation (FAO) rate was measured in liver homogenates from HFD-fed PKD2$^{fl/fl}$ and PKD2$^{\Delta Hep}$ mice (n = 16 for PKD2$^{fl/fl}$ mice and n = 19 for PKD2$^{\Delta Hep}$ mice). Values are mean ± SEM. *p < 0.05 *versus* PKD2$^{fl/fl}$ mice according to Student's t-test. ***D.*** *De novo* lipogenesis was evaluated in livers from HFD-fed PKD2$^{fl/fl}$ and PKD2$^{\Delta Hep}$ mice by [^{3}H]-acetate incorporation and FAs and TGs were analyzed (FA, n = 8 for PKD2$^{fl/fl}$ mice and n = 11 for PKD2$^{\Delta Hep}$ mice; TG, n = 8 for PKD2$^{fl/fl}$ mice and n = 11 for PKD2$^{\Delta Hep}$ mice). Values are mean ± SEM. ***E.*** Protein levels of pAMPK, pACC and FAS in liver extracts from HFD-fed PKD2$^{fl/fl}$ or PKD2$^{\Delta Hep}$ mice. Total AMPK, ACC and Vinculin were used as loading controls. Densitometric quantification of pAMPK and pACC protein levels. Values are mean ± SEM (pACC and pAMPK, n = 13 for PKD2$^{fl/fl}$ mice and n = 11 for PKD2$^{\Delta Hep}$ mice; FAS, n = 7).

levels are achieved 5 min after insulin stimulation, being this time-point the most optimal to find differential responses among genotypes. In fact, CRT0066101-pretreated Huh7 and Huh6 human hepatic cells also showed enhanced AKT phosphorylation at this time-period, whereas in the study of Xiao et al. AKT phosphorylation in Hepa1-6 cells was analyzed after a longer stimulation (15 min).

Tissue-specific disruption of insulin signaling has provided a powerful approach to dissect the critical nodes of this cascade, as well as to sort out direct and indirect effects [58,59]. Herein, we have demonstrated that hepatocyte-specific PKD2 deletion potentiates proximal insulin signaling events such as IRS1 Tyr phosphorylation, thereby enhancing downstream AKT activation. This effect occurs in hepatocytes from both CHD- and HFD-fed mice. In line with the *in vitro* results, higher insulin sensitivity manifested by reduced AUC in both ITT and PTT, as well as by enhanced phosphorylation levels of AKT and its downstream targets GSK3α/β, FOXO1 and ribosomal protein S6 was found in HFD-fed PKD2$^{\Delta Hep}$ mice when compared to their PKD2$^{fl/fl}$ counterparts. Despite enhanced insulin signaling in HFD-fed PKD2$^{\Delta Hep}$ mice upon an exogenous insulin challenge, under basal conditions hepatic glycogen levels did not differ between genotypes although glycogen content was elevaled in livers from PKD2$^{\Delta Hep}$ mice fed a CHD compared to PKD2$^{fl/fl}$ mice, pointing to a higher ability of those mice to store glycogen, an indicative of enhanced insulin action in hepatocytes. Conversely, hepatocyte-overexpression of a constitutively active version of PKD2 in mice fed a CHD, which resembles the increased PKD2 phosphorylation in mouse liver upon HFD, was sufficient to impair hepatic insulin signaling in absence of obesity supporting the pathophysiological relevance of our results. However, neither PKD2 deletion nor overexpression in hepatocytes impacted on insulin signaling in skeletal muscle where PKD2 was not genetically modified, suggesting that PKD2 levels in hepatocytes need to be finely tuned to ensure adequate systemic insulin sensitivity. A clear example of this effect has been described in liver-specific IR knockout (LIRKO) mice in which hepatocyte inactivation of the IR is sufficient to induce systemic insulin resistance despite preserving an intact insulin signaling in skeletal muscle [58]. It is notheworthy to mention that in line with many studies supporting sex differences in insulin resistance [60], the beneficial effects of hepatocyte PKD2 deficiency on enhancing insulin signaling, as well as insulin and pyruvate tolerance in male mice were not found in female mice. These sex-specific differences could be due, at least in part, to the absence of changes in *Prkd2* gene expression or its activation in female mice receiving a HFD for 14 weeks.

Of relevance, the present study demonstrates that, despite the fact that hepatic PKD1 expression is marginal as reported by Mayer et al. [22] and confirmed herein, unexpectedly, its deficiency in hepatocytes upregulates PKD2, and this might be an explanation for the impairment of insulin signaling in PKD1-deficient hepatocytes. These data enable us to postulate, on the one hand, that PKD1 and PKD2, despite their structural similarities [10,12,61], are not redundant in the liver and, on the other, that PKD2 likely compensates the loss of PKD1 in hepatocytes. Although most studies suggest that PKDs act in a functionally redundant manner [25,26,62,63], the antithetical role for PKD1 *versus* PKD2/PKD3 has also been reported, for instance, in the control of cell proliferation of certain cancer cells [64], supporting isoform-specific PKD responses depending on the cellular context [65,66].

Regarding PKD2 and PKD3, their overactivation (PKD3 in Mayer et al. [22] and PKD2 herein) is sufficient to impair insulin signaling in the liver. Instead, deletion of either PKD3 [22] or PKD2 enhances insulin sensitivity although it will be necessary to delete both isoforms to decipher if their individual deletion would be sufficient to reach a maximal effect on the enhancement of insulin signaling. This interesting issue will require further investigation.

Surprisingly, even though PKD3$^{\Delta Hep}$ mice displayed enhanced systemic insulin sensitivity, they presented higher TG and cholesterol accumulation in the liver after long-term (24 weeks) HFD administration due to the upregulation of lipogenic and cholesterol synthesis-related gene expression in hepatocytes [22]. At the molecular level, PKD3 deficiency increased insulin-induced AKT phosphorylation in hepatocytes; however, the negative crosstalk of PKD3 activation on the critical nodes of insulin signaling upstream AKT, particularly on IRS1 phosphorylation, was not elucidated in the study of Mayer et al. Also, since PKD3 is the most abundant PKD in the liver, its deletion in hepatocytes might rewire hepatic metabolism resulting in metabolic alterations such as enhanced steatosis and hypercholesterolemia that might cause metabolic syndrome in the long-term. Further, the specific role of PKD3 in restraining hepatic lipogenesis was reinforced by the treatment of PKD3$^{\Delta Hep}$ mice with CRT0066101, which inhibits the two remaining PKD isoforms, showing not further enhancement of the lipogenic expression profile by inhibiting PKD2 since, as stated above, hepatocyte PKD1 levels are marginal [22]. Additionally, we have provided results into whether other kinases rather than PKDs, might compensate for the loss of PKD2 in hepatocytes. In this regard, phosphorylation levels of protein kinases such as IKKα/β, JNK1/2 or ERK1/2 that block insulin signaling at the level of IRS1 [48–51], were similar in PKD2$^{fl/fl}$ and PKD2$^{\Delta Hep}$ hepatocytes. Alltogether, our findings support the relevance of PKD2 in the modulation of hepatic insulin signaling since its deficiency cannot be compensated by other kinases targeting IRS1.

It is well established that under physiological conditions insulin signaling, particularly AKT, controls hepatic lipogenesis [67]. Paradoxically, increased *de novo* lipogenesis is also a feature of insulin resistance in which insulin fails to suppress hepatic glucose production, but yet still augments or sustains *de novo* lipogenesis. This phenomenon is known as selective insulin resistance, pointing to distinct insulin sensitive pathways that independently modulate glucose and lipid metabolism [68]. In our settings of obesity-linked insulin resistance, the enhancement in phosphorylation of AKT and its downstream targets in the liver from PKD2$^{\Delta Hep}$ mice is not associated with elevated in *de novo* lipogenesis. Conversely, in the case of PKD3$^{\Delta Hep}$ mice fed a HFD for 24 weeks that also showed higher AKT phosphorylation in the liver and retained insulin sensitivity regarding glucose homeostasis, those mice presented a marked increase in hepatic lipogenesis, a feature of selective insulin resistance, pointing to substantial differences between PKD2 and PKD3 in modulating lipid metabolism under obesogenic conditions that deserve further investigation. Moreover, the results on the evaluation of lipid metabolic fluxes in the liver of HFD-fed PKD2$^{\Delta Hep}$ mice evidenced an increase in FAO without changes in the total pool of DG and TG, although the lipidomic analysis revealed an increase in 6 DG species. Moreover, although total PL content was not altered in the liver from PKD2$^{\Delta Hep}$ mice, several PL species were decreased. Altogether, these results suggest a scenario of lipid species remodeling possibly mediated by activation of phospholipases that provide, among others, FAs as substrates to fuel FAO, but without alterations in total TG, DG and PL content, as well as in the NAS score. Interestingly, mice deficient in type V secretory phospholipase A2 (sPLA2-V) exhibited increased adiposity, insulin resistance, hepatic steatosis and hyperlipidemia [69]. Therefore, it is tempting to speculate that in HFD-fed PKD2$^{\Delta Hep}$ mice the lipid remodeling might be beneficial in the long-term to slow down the progresion to a more severe MASLD stage. In addition, the decrease in plasma free FAs

could be an indicative of increased insulin sensitivity in white adipose tissue by restraining lipolysis. Overall, our results suggest that deletion of PKD2 rather than PKD3 is likely a more appropriated strategy to enhance insulin sensitivity without further causing potential metabolic rearrangements in hepatic lipid metabolism that might be deleterious in the long-term.

Multiple studies have demonstrated that IRS1 serine phosphorylation is directly related to the impairment of its tyrosine phosphorylation, thereby blocking insulin signaling [46,47,49]. Particularly, the work from Mothe and Van Obberghen [70] highlights Ser612, which is nearby the phosphatidylinositol 3-kinase (PI3K) binding motif Tyr608XXM, as a key negative modulator of IRS1 tyrosine phosphorylation and the activity of PI3K upon insulin stimulation. Also, an inverse relationship between IRS1 Ser612 phosphorylation and AKT activation has been demonstrated in HepG2 cells treated with a natural compound derived from quercetin [71]. However, controversy on the *in vivo* relevance of IRS1 serine phosphorylation as a negative modulator of AKT and hence, glucose homeostasis, has been raised by the study of Copps and co-workers [72]. They showed IRS1 Ser302-independent effects in the negative modulation of AKT phosphorylation by the feed-back driven by mTORC1/S6K. However, these results do not contradict our data because we postulate that PKD2, alone or within a signaling complex, is likely responsible of phosphorylating IRS1 at Ser612 and maybe at additional serine residues. Our data are supported by *in vivo* evidences of decreased IRS1 Ser612 phosphorylation and increased IRS1-mediated AKT downstream insulin signaling together with an improvement of systemic insulin sensitivity in obese mice lacking PKD2 in hepatocytes. More closely related to our study, in HEK293T cells, Ser612 in IRS1 has been shown to be phosphorylated upon PKC activation by phorbol 12-myristate 13-acetate (PMA) [73] and, importantly, mutation of this site protected HEK293T against PMA-induced insulin resistance. In addition, Kahn and colleagues [74] demonstrated decreased IRS1 Ser612 phosphorylation in the liver of mice lacking *Prkcd*, which encodes the atypical PKCδ, reflecting IRS1 targeting by PKCδ. Since on the one hand, other studies also reported impairments in insulin signaling via PKC-mediated IRS1 serine phosphorylation [75,76] and, on the other, PKD is a downstream target of PKCs [77], we cannot exclude the existence of a PKC/PKD/IRS1 axis in the modulation of insulin effector cascades. It is noteworthy to highlight that we have provided new molecular insights on the negative modulation of hepatic insulin signaling likely mediated by an association of PKD2 with IRS1. At present, we cannot address whether IRS1 is a direct PKD2 substrate due to the lack of the consensus PKD phosphorylation motif [78] in IRS1. However, our results show that PKD2 is present at the plasma membrane and IRS1 Ser612 phosphorylation is reduced when PKD2 is absent, supporting its relevant contribution to the modulation of IRS1 activity. In this context, an association of IRS1-PKD1 has been reported in MCF-7 cells in response to growth factor stimulation, without modifying IRS1 serine phosphorylation [79]. The authors of this study argued that the IRS1-PKD1 association might reduce the affinity of the latter for insulin-like growth factor-1 receptor, thereby decreasing its subsequent tyrosine phosphorylation. In this regard, our results point to a modulation of IRS1 activity by PKD2-mediated serine phosphorylation rather than an effect on IR kinase activity.

Regarding the traslational relevance of our results, it is noteworthy to highlight that there are no PKD-related drugs currently entering clinical trials for cancer or metabolic diseases [80]. Recently, specific pan-PKD inhibitors have been discovered, including CRT0066101 used in this study. These compounds have shown therapeutic effects in preclinical studies and are promising drug candidates [81–83]. However, their use in the clinic is limited by the tissue- and isoform-specific roles of PKDs in different pathological contexts or even in the same disease, as shown herein and in other studies [19–22,24]. Thus, more research is needed to overcome these limitations and offer more precise treatments.

5. CONCLUSIONS

In conclusion, this study has unraveled new molecular insights on PKD2 as a negative modulator of hepatocyte insulin signaling and a potential therapeutic candidate to tackle insulin resistance in the liver.

FUNDING

This work was funded by grants PID2023-150994OB-I00 funded by MICIU/AEI/10.13039/501100011033 and by "ERDF/EU" to PR; PID2021-122766OB-100 funded by MICIU/AEI/10.13039/501100011033 and by "ERDF/EU" to AMV; PID2020-115218RB-I00 funded by MICIU/AEI/10.13039/501100011033 and by "ERDF A way of making Europe" to TI; PID2021-124425OB-I00 funded by MICIU/AEI/10.13039/501100011033 and by "ERDF/EU" to PA; PDC2021-121147-I00 funded by MICIU/AEI/10.13039/501100011033 and by the "European Union NextGenerationEU/PRTR" to GS. We also acknowledge grants PI20/00837 to CG-M, PMP21/00057 to GS and PA, and PI22/01968 to ÁG-R funded by Instituto de Salud Carlos III/FEDER (Spain), and IT1476-22 funded by Basque Government, Department of Education (Spain) to PA, grants P2022/BMD-7227 funded by Comunidad de Madrid (Spain) to AMV and AG and funding from CIBERDEM (ISCIII, Spain) to AMV and CIBERNED (ISCIII, Spain) to TI, including PR and JPU research contracts, respectively. CNIC is a Severo Ochoa Center of Excellence (grant CEX2020-001041-S funded by MICIN/AEI/10.13039/501100011033). EC-L is funded by Comunidad de Madrid and Fondo Social Europeo (ref. PEJ-2020-AI/BMD-18301).

CRediT AUTHORSHIP CONTRIBUTION STATEMENT

Patricia Rada: Writing — review & editing, Writing — original draft, Visualization, Validation, Supervision, Methodology, Investigation, Funding acquisition, Formal analysis, Conceptualization. **Elena Carceller-López:** Writing — review & editing, Visualization, Methodology, Investigation. **Ana B. Hitos:** Writing — review & editing, Methodology, Investigation. **Beatriz Gómez-Santos:** Writing — review & editing, Methodology, Investigation, Formal analysis, Data curation. **Constanza Fernández-Hernández:** Writing — review & editing, Visualization, Methodology, Investigation. **Esther Rey:** Writing — review & editing, Methodology, Investigation. **Julia Pose-Utrilla:** Writing — review & editing, Methodology, Investigation. **Carmelo García-Monzón:** Writing — review & editing, Visualization, Methodology, Investigation, Funding acquisition, Formal analysis. **Águeda González-Rodríguez:** Writing — review & editing, Methodology, Investigation, Funding acquisition. **Guadalupe Sabio:** Writing — review & editing, Resources, Methodology, Investigation, Funding acquisition, Formal analysis. **Antonia García:** Writing — review & editing, Visualization, Validation, Supervision, Resources, Methodology, Investigation, Funding acquisition, Formal analysis, Data curation. **Patricia Aspichueta:** Writing — review & editing, Visualization, Validation, Resources, Methodology, Investigation, Funding acquisition, Formal analysis, Data curation, Conceptualization. **Teresa Iglesias:** Writing — review & editing, Methodology, Investigation, Funding acquisition, Formal analysis. **Ángela M.**

Valverde: Writing — review & editing, Writing — original draft, Visualization, Validation, Resources, Project administration, Methodology, Investigation, Funding acquisition, Formal analysis, Conceptualization.

ACKNOWLEDGEMENT

The authors would like to thank all members of AMV's laboratory for the helpful discussion. We also acknowledge Á. Montes-San Lorenzo (IIBM, CSIC) for the technical support. The graphical abstract was created with http://Biorender.com.

DECLARATION OF COMPETING INTEREST

The authors declare that they have no known competing financial interests or personal relationships that could have appeared to influence the work reported in this paper.

APPENDIX A. SUPPLEMENTARY DATA

Supplementary data to this article can be found online at https://doi.org/10.1016/j.molmet.2024.102045.

DATA AVAILABILITY

Data will be made available on request.

REFERENCES

[1] DeFronzo RA, Simonson D, Ferrannini E. Hepatic and peripheral insulin resistance: a common feature of type 2 (non-insulin-dependent) and type 1 (insulin-dependent) diabetes mellitus. Diabetologia 1982;23(4):313—9. https://doi.org/10.1007/BF00253736.

[2] Kim CH, Younossi ZM. Nonalcoholic fatty liver disease: a manifestation of the metabolic syndrome. Cleve Clin J Med 2008;75(10):721—8. https://doi.org/10.3949/ccjm.75.10.721.

[3] Rinella ME, Lazarus JV, Ratziu V, Francque SM, Sanyal AJ, Kanwal F, et al. A multisociety Delphi consensus statement on new fatty liver disease nomenclature. Hepatology 2023;78(6):1966—86. https://doi.org/10.1097/HEP.0000000000000520.

[4] Rinella ME, Lazarus JV, Ratziu V, Francque SM, Sanyal AJ, Kanwal F, et al. A multisociety Delphi consensus statement on new fatty liver disease nomenclature. J Hepatol 2023;79(6):1542—56. https://doi.org/10.1016/j.jhep.2023.06.003.

[5] Manning G, Whyte DB, Martinez R, Hunter T, Sudarsanam S. The protein kinase complement of the human genome. Science 2002;298(5600):1912—34. https://doi.org/10.1126/science.1075762.

[6] Valverde AM, Sinnett-Smith J, Van Lint J, Rozengurt E. Molecular cloning and characterization of protein kinase D: a target for diacylglycerol and phorbol esters with a distinctive catalytic domain. Proc Natl Acad Sci USA 1994;91(18):8572—6. https://doi.org/10.1073/pnas.91.18.8572.

[7] Hayashi A, Seki N, Hattori A, Kozuma S, Saito T. PKCν, a new member of the protein kinase C family, composes a fourth subfamily with PKCμ1The nucleotide sequence data reported in this paper have been deposited in the DDBJ, EMBL and GenBank databases under the accession number AB015982.1. Biochim Biophys Acta Mol Cell Res 1999;1450(1):99—106. https://doi.org/10.1016/S0167-4889(99)00040-3.

[8] Sturany S, Van Lint J, Müller F, Wilda M, Hameister H, Höcker M, et al. Molecular cloning and characterization of the human protein kinase D2. J Biol Chem 2001;276(5):3310—8. https://doi.org/10.1074/jbc.M008719200.

[9] Johannes FJ, Prestle J, Eis S, Oberhagemann P, Pfizenmaier K. PKCu is a novel, atypical member of the protein kinase C family. J Biol Chem 1994;269(8):6140—8.

[10] Matthews SA, Navarro MN, Sinclair LV, Emslie E, Feijoo-Carnero C, Cantrell DA. Unique functions for protein kinase D1 and protein kinase D2 in mammalian cells. Biochem J 2010;432(1):153—63. https://doi.org/10.1042/BJ20101188.

[11] Fu Y, Rubin CS. Protein kinase D: coupling extracellular stimuli to the regulation of cell physiology. EMBO Rep 2011;12(8):785—96. https://doi.org/10.1038/embor.2011.139.

[12] Ellwanger K, Hausser A. Physiological functions of protein kinase D *in vivo*. IUBMB Life 2013;65(2):98—107. https://doi.org/10.1002/iub.1116.

[13] Sinnett-Smith J, Zhukova E, Rey O, Rozengurt E. Protein kinase D2 potentiates MEK/ERK/RSK signaling, c-Fos accumulation and DNA synthesis induced by bombesin in Swiss 3T3 cells. J Cell Physiol 2007;211(3):781—90. https://doi.org/10.1002/jcp.20984.

[14] Samuel VT, Liu Z-X, Qu X, Elder BD, Bilz S, Befroy D, et al. Mechanism of hepatic insulin resistance in non-alcoholic fatty liver disease. J Biol Chem 2004;279(31):32345—53. https://doi.org/10.1074/jbc.M313478200.

[15] Donnelly KL, Smith CI, Schwarzenberg SJ, Jessurun J, Boldt MD, Parks EJ. Sources of fatty acids stored in liver and secreted via lipoproteins in patients with nonalcoholic fatty liver disease. J Clin Invest 2005;115(5):1343—51. https://doi.org/10.1172/JCI23621.

[16] Nagai Y, Yonemitsu S, Erion DM, Iwasaki T, Stark R, Weismann D, et al. The role of peroxisome proliferator-activated receptor γ coactivator-1 β in the pathogenesis of fructose-induced insulin resistance. Cell Metabol 2009;9(3):252—64. https://doi.org/10.1016/j.cmet.2009.01.011.

[17] Toriumi K, Horikoshi Y, Yoshiyuki Osamura R, Yamamoto Y, Nakamura N, Takekoshi S. Carbon tetrachloride-induced hepatic injury through formation of oxidized diacylglycerol and activation of the PKC/NF-κB pathway. Lab Invest 2013;93(2):218—29. https://doi.org/10.1038/labinvest.2012.145.

[18] Yoon S, Maruyama Y, Kazusaka A, Fujita S. Accumulation of diacylglycerol induced by CCl4-derived radicals in rat liver membrane and its inhibition with radical trapping reagent–FT-IR spectroscopic and HPLC chromatographic observations. Jpn J Vet Res 2000;47(3—4):135—44.

[19] Sumara G, Formentini I, Collins S, Sumara I, Windak R, Bodenmiller B, et al. Regulation of PKD by the MAPK p38δ in insulin secretion and glucose homeostasis. Cell 2009;136(2):235—48. https://doi.org/10.1016/j.cell.2008.11.018.

[20] Bergeron V, Ghislain J, Vivot K, Tamarina N, Philipson LH, Fielitz J, et al. Deletion of protein kinase D1 in pancreatic β-cells impairs insulin secretion in high-fat diet—fed mice. Diabetes 2018;67(1):71—7. https://doi.org/10.2337/db17-0982.

[21] Löffler MC, Mayer AE, Trujillo Viera J, Loza Valdes A, El-Merahbi R, Ade CP, et al. Protein kinase D1 deletion in adipocytes enhances energy dissipation and protects against adiposity. EMBO J 2018;37(22). https://doi.org/10.15252/embj.201899182.

[22] Mayer AE, Löffler MC, Loza Valdés AE, Schmitz W, El-Merahbi R, Viera JT, et al. The kinase PKD3 provides negative feedback on cholesterol and triglyceride synthesis by suppressing insulin signaling. Sci Signal 2019;12(593):eaav9150. https://doi.org/10.1126/scisignal.aav9150.

[23] Xiao Y, Wang C, Chen J-Y, Lu F, Wang J, Hou N, et al. Deficiency of PRKD2 triggers hyperinsulinemia and metabolic disorders. Nat Commun 2015;9(1):2015. https://doi.org/10.1038/s41467-018-04352-z.

[24] Trujillo-Viera J, El-Merahbi R, Schmidt V, Karwen T, Loza-Valdes A, Strohmeyer A, et al. Protein Kinase D2 drives chylomicron-mediated lipid transport in the intestine and promotes obesity. EMBO Mol Med 2021;13(5):e13548. https://doi.org/10.15252/emmm.202013548.

[25] Avriyanti E, Atik N, Kunii M, Furumoto N, Iwano T, Yoshimura S, et al. Functional redundancy of protein kinase D1 and protein kinase D2 in neuronal polarity. Neurosci Res 2015;95:12—20. https://doi.org/10.1016/j.neures.2015.01.007.

[26] Atik N, Kunii M, Avriyanti E, Furumoto N, Inami K, Yoshimura S, et al. The role of PKD in cell polarity, biosynthetic pathways, and organelle/F-actin distribution. Cell Struct Funct 2014;39(1):61—77. https://doi.org/10.1247/csf.13020.

[27] Pose-Utrilla J, García-Guerra L, Del Puerto A, Martín A, Jurado-Arjona J, De León-Reyes NS, et al. Excitotoxic inactivation of constitutive oxidative stress detoxification pathway in neurons can be rescued by PKD1. Nat Commun 2017;8(1):2275. https://doi.org/10.1038/s41467-017-02322-5.

[28] Fielitz J, Kim M-S, Shelton JM, Qi X, Hill JA, Richardson JA, et al. Requirement of protein kinase D1 for pathological cardiac remodeling. Proc Natl Acad Sci USA 2008;105(8):3059—63. https://doi.org/10.1073/pnas.0712265105.

[29] Kleiner DE, Brunt EM, Van Natta M, Behling C, Contos MJ, Cummings OW, et al. Design and validation of a histological scoring system for nonalcoholic fatty liver disease. Hepatology (Baltimore, Md 2005;41(6):1313—21. https://doi.org/10.1002/hep.20701.

[30] Gonzalez-Riano C, Gradillas A, Barbas C. Exploiting the formation of adducts in mobile phases with ammonium fluoride for the enhancement of annotation in liquid chromatography-high resolution mass spectrometry based lipidomics. Journal of Chromatography Open 2021;1:100018. https://doi.org/10.1016/j.jcoa.2021.100018.

[31] N.d. MetaboAnalyst. https://www.metaboanalyst.ca/. accessed January 17, 2024.

[32] Folch J, Lees M, Sloane Stanley GH. A simple method for the isolation and purification of total lipides from animal tissues. J Biol Chem 1957;226(1):497—509.

[33] Ruiz JI, Ochoa B. Quantification in the subnanomolar range of phospholipids and neutral lipids by monodimensional thin-layer chromatography and image analysis. JLR (J Lipid Res) 1997;38(7):1482—9.

[34] Sáenz de Urturi D, Buqué X, Porteiro B, Folgueira C, Mora A, Delgado TC, et al. Methionine adenosyltransferase 1a antisense oligonucleotides activate the liver-brown adipose tissue axis preventing obesity and associated hepatosteatosis. Nat Commun 2022;13(1):1096. https://doi.org/10.1038/s41467-022-28749-z.

[35] Gómez-Santos B, Saenz de Urturi D, Nuñez-García M, Gonzalez-Romero F, Buque X, Aurrekoetxea I, et al. Liver osteopontin is required to prevent the progression of age-related nonalcoholic fatty liver disease. Aging Cell 2020;19(8):e13183. https://doi.org/10.1111/acel.13183.

[36] Nassir F, Adewole OL, Brunt EM, Abumrad NA. CD36 deletion reduces VLDL secretion, modulates liver prostaglandins, and exacerbates hepatic steatosis in ob/ob mice. JLR (J Lipid Res) 2013;54(11):2988—97. https://doi.org/10.1194/jlr.M037812.

[37] Rada P, Lamballe F, Carceller-López E, Hitos AB, Sequera C, Maina F, et al. Enhanced wild-type MET receptor levels in mouse hepatocytes attenuates insulin-mediated signaling. Cells 2022;11(5):793. https://doi.org/10.3390/cells11050793.

[38] Pardo V, González-Rodríguez Á, Guijas C, Balsinde J, Valverde ÁM. Opposite cross-talk by oleate and palmitate on insulin signaling in hepatocytes through macrophage activation. J Biol Chem 2015;290(18):11663—77. https://doi.org/10.1074/jbc.M115.649483.

[39] Schindelin J, Arganda-Carreras I, Frise E, Kaynig V, Longair M, Pietzsch T, et al. Fiji: an open-source platform for biological-image analysis. Nat Methods 2012;9(7):676—82. https://doi.org/10.1038/nmeth.2019.

[40] Garcia-Martinez I, Alen R, Pereira L, Povo-Retana A, Astudillo AM, Hitos AB, et al. Saturated fatty acid-enriched small extracellular vesicles mediate a crosstalk inducing liver inflammation and hepatocyte insulin resistance. JHEP Reports 2023;5(8):100756. https://doi.org/10.1016/j.jhepr.2023.100756.

[41] Pescador N, Francisco V, Vázquez P, Esquinas EM, González-Páramos C, Valdecantos MP, et al. Metformin reduces macrophage HIF1α-dependent proinflammatory signaling to restore brown adipocyte function in vitro. Redox Biol 2021;48:102171. https://doi.org/10.1016/j.redox.2021.102171.

[42] Escalona-Garrido C, Vázquez P, Mera P, Zagmutt S, García-Casarrubios E, Montero-Pedrazuela A, et al. Moderate SIRT1 overexpression protects against brown adipose tissue inflammation. Mol Metabol 2020;42:101097. https://doi.org/10.1016/j.molmet.2020.101097.

[43] Gonzalez-Rellan MJ, Fondevila MF, Fernandez U, Rodríguez A, Varela-Rey M, Veyrat-Durebex C, et al. O-GlcNAcylated p53 in the liver modulates hepatic glucose production. Nat Commun 2021;12(1):5068. https://doi.org/10.1038/s41467-021-25390-0.

[44] Wei N, Chu E, Wipf P, Schmitz JC. Protein kinase d as a potential chemotherapeutic target for colorectal cancer. Mol Cancer Therapeut 2014;13(5):1130—41. https://doi.org/10.1158/1535-7163.MCT-13-0880.

[45] Gilles P, Voets L, Van Lint J, De Borggraeve WM. Developments in the discovery and design of protein kinase D inhibitors. ChemMedChem 2021;16(14):2158—71. https://doi.org/10.1002/cmdc.202100110.

[46] Pederson TM, Kramer DL, Rondinone CM. Serine/threonine phosphorylation of IRS-1 triggers its degradation. Diabetes 2001;50(1):24—31. https://doi.org/10.2337/diabetes.50.1.24.

[47] Schmitz-Peiffer C, Whitehead J. IRS-1 regulation in health and disease. IUBMB Life 2003;55(7):367—74. https://doi.org/10.1080/1521654031000138569.

[48] Nakatani Y, Kaneto H, Kawamori D, Hatazaki M, Miyatsuka T, Matsuoka T-A, et al. Modulation of the JNK pathway in liver affects insulin resistance status. J Biol Chem 2004;279(44):45803—9. https://doi.org/10.1074/jbc.M406963200.

[49] Copps KD, White MF. Regulation of insulin sensitivity by serine/threonine phosphorylation of insulin receptor substrate proteins IRS1 and IRS2. Diabetologia 2012;55(10):2565—82. https://doi.org/10.1007/s00125-012-2644-8.

[50] Fritsche L, Neukamm SS, Lehmann R, Kremmer E, Hennige AM, Hunder-Gugel A, et al. Insulin-induced serine phosphorylation of IRS-2 via ERK1/2 and mTOR: studies on the function of Ser675 and Ser907. Am J Physiol Endocrinol Metab 2011;300(5):E824—36. https://doi.org/10.1152/ajpendo.00409.2010.

[51] Gao Z, Hwang D, Bataille F, Lefevre M, York D, Quon MJ, et al. Serine phosphorylation of insulin receptor substrate 1 by inhibitor kappa B kinase complex. J Biol Chem 2002;277(50):48115—21. https://doi.org/10.1074/jbc.M209459200.

[52] Samuel VT, Shulman GI. Mechanisms for insulin resistance: common threads and missing links. Cell 2012;148(5):852—71. https://doi.org/10.1016/j.cell.2012.02.017.

[53] Kolczynska K, Loza-Valdes A, Hawro I, Sumara G. Diacylglycerol-evoked activation of PKC and PKD isoforms in regulation of glucose and lipid metabolism: a review. Lipids Health Dis 2020;19(1):113. https://doi.org/10.1186/s12944-020-01286-8.

[54] Jiao Y, Williams A, Wei N. Quercetin ameliorated insulin resistance via regulating METTL3-mediated N6-methyladenosine modification of PRKD2 mRNA in skeletal muscle and C2C12 myocyte cell line. Nutr Metabol Cardiovasc Dis: Nutr Metabol Cardiovasc Dis 2022;32(11):2655—68. https://doi.org/10.1016/j.numecd.2022.06.019.

[55] Huggett ZJ, Smith A, De Vivo N, Gomez D, Jethwa P, Brameld JM, et al. A comparison of primary human hepatocytes and hepatoma cell lines to model the effects of fatty acids, fructose and glucose on liver cell lipid accumulation. Nutrients 2022;15(1):40. https://doi.org/10.3390/nu15010040.

[56] Molinaro A, Becattini B, Solinas G. Insulin signaling and glucose metabolism in different hepatoma cell lines deviate from hepatocyte physiology toward a convergent aberrant phenotype. Sci Rep 2020;10(1):12031. https://doi.org/10.1038/s41598-020-68721-9.

[57] Huang MT, Veech RL. Role of the direct and indirect pathways for glycogen synthesis in rat liver in the postprandial state. J Clin Investig 1988;81(3):872—8. https://doi.org/10.1172/JCI113397.

[58] Michael MD, Kulkarni RN, Postic C, Previs SF, Shulman GI, Magnuson MA, et al. Loss of insulin signaling in hepatocytes leads to severe insulin resistance and progressive hepatic dysfunction. Mol Cell 2000;6(1):87—97.

[59] Kahn CR. The Gordon Wilson Lecture. Lessons about the control of glucose homeostasis and the pathogenesis of diabetes from knockout mice. Trans Am Clin Climatol Assoc 2003;114:125—48.

[60] Gado M, Tsaousidou E, Bornstein SR, Perakakis N. Sex-based differences in insulin resistance. J Endocrinol 2024;261(1):e230245. https://doi.org/10.1530/JOE-23-0245.

[61] Cobbaut M, Van Lint J. Function and regulation of protein kinase D in oxidative stress: a tale of isoforms. Oxid Med Cell Longev 2018;2018:2138502. https://doi.org/10.1155/2018/2138502.

[62] Yeaman C, Ayala MI, Wright JR, Bard F, Bossard C, Ang A, et al. Protein kinase D regulates basolateral membrane protein exit from trans-Golgi network. Nat Cell Biol 2004;6(2):106–12. https://doi.org/10.1038/ncb1090.

[63] Mihailovic T, Marx M, Auer A, Van Lint J, Schmid M, Weber C, et al. Protein kinase D2 mediates activation of nuclear factor κB by Bcr-Abl in Bcr-Abl+ human myeloid leukemia cells. Cancer Res 2004;64(24):8939–44. https://doi.org/10.1158/0008-5472.CAN-04-0981.

[64] Roy A, Ye J, Deng F, Wang QJ. Protein kinase D signaling in cancer: a friend or foe? Biochim Biophys Acta Rev Cancer 2017;1868(1):283–94. https://doi.org/10.1016/j.bbcan.2017.05.008.

[65] Qiu W, Steinberg SF. Phos-tag SDS-PAGE resolves agonist- and isoform-specific activation patterns for PKD2 and PKD3 in cardiomyocytes and cardiac fibroblasts. J Mol Cell Cardiol 2016;99:14–22. https://doi.org/10.1016/j.yjmcc.2016.08.005.

[66] Steinberg SF. Decoding the cardiac actions of protein kinase D isoforms. Mol Pharmacol 2021;100(6):558–67. https://doi.org/10.1124/molpharm.121.000341.

[67] Uehara K, Santoleri D, Whitlock AEG, Titchenell PM. Insulin regulation of hepatic lipid homeostasis. Compr Physiol 2023;13(3):4785–809. https://doi.org/10.1002/cphy.c220015.

[68] Brown MS, Goldstein JL. Selective versus total insulin resistance: a pathogenic paradox. Cell Metabol 2008;7(2):95–6. https://doi.org/10.1016/j.cmet.2007.12.009.

[69] Sato H, Taketomi Y, Ushida A, Isogai Y, Kojima T, Hirabayashi T, et al. The adipocyte-inducible secreted phospholipases PLA2G5 and PLA2G2E play distinct roles in obesity. Cell Metabol 2014;20(1):119–32. https://doi.org/10.1016/j.cmet.2014.05.002.

[70] Mothe I, Van Obberghen E. Phosphorylation of insulin receptor substrate-1 on multiple serine residues, 612, 632, 662, and 731, modulates insulin action. J Biol Chem 1996;271(19):11222–7. https://doi.org/10.1074/jbc.271.19.11222.

[71] Tang P, Tang Y, Liu Y, He B, Shen X, Zhang Z-J, et al. Quercetin-3-*O*-α-L-arabinopyranosyl-(1→2)-β-D-glucopyranoside isolated from *Eucommia ulmoides* leaf relieves insulin resistance in HepG2 cells *via* the IRS-1/PI3K/Akt/GSK-3β pathway. Biol Pharm Bull 2023;46(2):219–29. https://doi.org/10.1248/bpb.b22-00597.

[72] Copps KD, Hançer NJ, Qiu W, White MF. Serine 302 phosphorylation of mouse insulin receptor substrate 1 (IRS1) is dispensable for normal insulin signaling and feedback regulation by hepatic S6 kinase. J Biol Chem 2016;291(16):8602–17. https://doi.org/10.1074/jbc.M116.714915.

[73] De Fea K, Roth RA. Protein kinase C modulation of insulin receptor substrate-1 tyrosine phosphorylation requires serine 612. Biochemistry 1997;36(42):12939–47. https://doi.org/10.1021/bi971157f.

[74] Bezy O, Tran TT, Pihlajamäki J, Suzuki R, Emanuelli B, Winnay J, et al. PKCδ regulates hepatic insulin sensitivity and hepatosteatosis in mice and humans. J Clin Investig 2011;121(6):2504–17. https://doi.org/10.1172/JCI46045.

[75] Yu C, Chen Y, Cline GW, Zhang D, Zong H, Wang Y, et al. Mechanism by which fatty acids inhibit insulin activation of insulin receptor substrate-1 (IRS-1)-associated phosphatidylinositol 3-kinase activity in muscle. J Biol Chem 2002;277(52):50230–6. https://doi.org/10.1074/jbc.M200958200.

[76] Kim JK, Fillmore JJ, Sunshine MJ, Albrecht B, Higashimori T, Kim D-W, et al. PKC-theta knockout mice are protected from fat-induced insulin resistance. J Clin Investig 2004;114(6):823–7. https://doi.org/10.1172/JCI22230.

[77] Zhang X, Connelly J, Chao Y, Wang QJ. Multifaceted functions of protein kinase D in pathological processes and human diseases. Biomolecules 2021;11(3):483. https://doi.org/10.3390/biom11030483.

[78] Iglesias T, Cabrera-Poch N, Mitchell MP, Naven TJ, Rozengurt E, Schiavo G. Identification and cloning of Kidins220, a novel neuronal substrate of protein kinase D. J Biol Chem 2000;275(51):40048–56. https://doi.org/10.1074/jbc.M005261200.

[79] Karam M, Lassarre C, Legay C, Ricort J-M. Phosphatidylinositol 3-kinase and protein kinase D1 specifically cooperate to negatively regulate the insulin-like growth factor signaling pathway. Biochim Biophys Acta Mol Cell Res 2012;1823(2):558–69. https://doi.org/10.1016/j.bbamcr.2011.12.007.

[80] Lv D, Chen H, Feng Y, Cui B, Kang Y, Zhang P, et al. Small-Molecule inhibitor targeting protein kinase D: a potential therapeutic strategy. Front Oncol 2021;11:680221. https://doi.org/10.3389/fonc.2021.680221.

[81] Sharlow ER, Giridhar KV, LaValle CR, Chen J, Leimgruber S, Barrett R, et al. Potent and selective disruption of protein kinase D functionality by a benzoxoloazepinolone. J Biol Chem 2008;283(48):33516–26. https://doi.org/10.1074/jbc.M805358200.

[82] Harikumar KB, Kunnumakkara AB, Ochi N, Tong Z, Deorukhkar A, Sung B, et al. A novel small-molecule inhibitor of protein kinase D blocks pancreatic cancer growth in vitro and in vivo. Mol Cancer Therapeut 2010;9(5):1136–46. https://doi.org/10.1158/1535-7163.MCT-09-1145.

[83] Tandon M, Salamoun JM, Carder EJ, Farber E, Xu S, Deng F, et al. SD-208, a novel protein kinase D inhibitor, blocks prostate cancer cell proliferation and tumor growth in vivo by inducing G2/M cell cycle arrest. PLoS One 2015;10(3):e0119346. https://doi.org/10.1371/journal.pone.0119346.

